Minerals Engineering 202 (2023) 108285

Contents lists available at ScienceDirect

Minerals Engineering

journal homepage: www.elsevier.com/locate/mineng

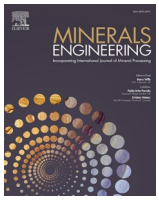

A study on the desulfurization of sulfidic mine tailings for the production of a sulfur-poor residue

Ana Luiza Coelho Braga de Carvalho [a,*], Victor Albuquerque de Carvalho [a], Rosie Blannin [b], Alexandra Gomez Escobar [c], Max Frenzel [b], Martin Rudolph [b], André Carlos Silva [d], Daniel Goldmann [a]

[a] Clausthal University of Technology. Walther-Nernst-Straße 9, 38678 Clausthal-Zellerfeld, Germany
[b] Helmholtz-Zentrum Dresden-Rossendorf (HZDR), Helmholtz Institute Freiberg for Resource Technology (HIF), Chemnitzer Straße 40, 09599 Freiberg, Germany
[c] Faculdade de Ciências, Instituto Dom Luiz, Universidade de Lisboa, Lisbon, Portugal
[d] Modelling and Mineral Processing Research Lab (LaMPPMin), Federal University of Catalão (UFCAT), 08 street 25, 75705-321 Catalão, GO, Brazil

ARTICLE INFO

Keywords:
Mine waste
Froth flotation
Sulfidic residues
Floc flotation
Ultrafine particles
Automated mineralogy

ABSTRACT

The mining industry generates large amounts of tailings every year. The most common destination for the tailings is deposition in tailings storage facilities (TSFs), which can have enormous dimensions. The management and storage of such large volumes of material pose many challenges in terms of dam stability and immobilization of hazardous contaminants that represent human-health and environmental risks, particularly for sulfide-containing materials. In addition, considerable amounts of precious and base metals can be lost in the tailings. Due to the economic value and growing industrial demand for precious and base metals, tailings may therefore be potential sources of secondary raw materials. This contribution investigates the flotation of pyrite-rich tailings, containing residual chalcopyrite, galena, and sphalerite, and high amounts of ultrafine particles. Flotation was used to recover the sulfide minerals and generate tailings with low sulfur content. The Cu-Pb-Zn-rich product could go to further treatment (e.g. (bio)hydrometallurgy) to recover the metals, while the low sulfur fraction could be used in the civil construction industry. Automated mineralogy (MLA) was used to provide quantitative mineralogical and textural data. Bench-scale experiments were performed by combining classic flotation and floc flotation (flotation of flocs of targeted minerals). Flotation of the material as received, as well as after classification into two fractions was performed. The samples as received and the coarser fraction (+37 μm) underwent classic flotation, while the finer fraction (−37 μm) was processed either by using the classic or the floc flotation approach. The flotation of the coarser particles provided higher sulfide recoveries, higher combined Cu-Pb-Zn grades in the concentrate (3.66 %), cleaner residues (1.6 % S), faster flotation rates, and reduced reagent consumption. Likewise, the results from the fine particle flotation allowed lower S content in the residues (3.4 % S) as compared to the flotation of the original material. The results of the use of floc flotation for the finer fraction show an increase in the mass pull with a slight increase in the recovery of sulfides. Overall, the development of a route to process the tailings proved to be promising and the use of a two-route approach indicates advantages as compared to a single route.

1. Introduction

The mining industry generates large amounts of waste every year. The overburden material that has to be removed to gain access to the ore is usually called waste rock and the residue generated after the mineral processing operations (i.e. crushing, grinding, and concentration) is referred to as tailings. The tailings consist of ore particles and processing effluents. Considering the enormous volumes of ore processed annually by the mining industry, and only a small percentage of this volume being recovered for further use (valuable minerals), tailings represent the

* Corresponding author.
E-mail addresses: alcbdc18@tu-clausthal.de (A.L.C.B. de Carvalho), vadc19@tu-clausthal.de (V.A. de Carvalho), r.blannin@hzdr.de (R. Blannin), agescobar@fc.ul.pt (A.G. Escobar), m.frenzel@hzdr.de (M. Frenzel), m.rudolph@hzdr.de (M. Rudolph), ancarsil@ufcat.edu.br (A.C. Silva), daniel.goldmann@tu-clausthal.de (D. Goldmann).

https://doi.org/10.1016/j.mineng.2023.108285
Received 14 November 2022; Received in revised form 27 July 2023; Accepted 30 July 2023

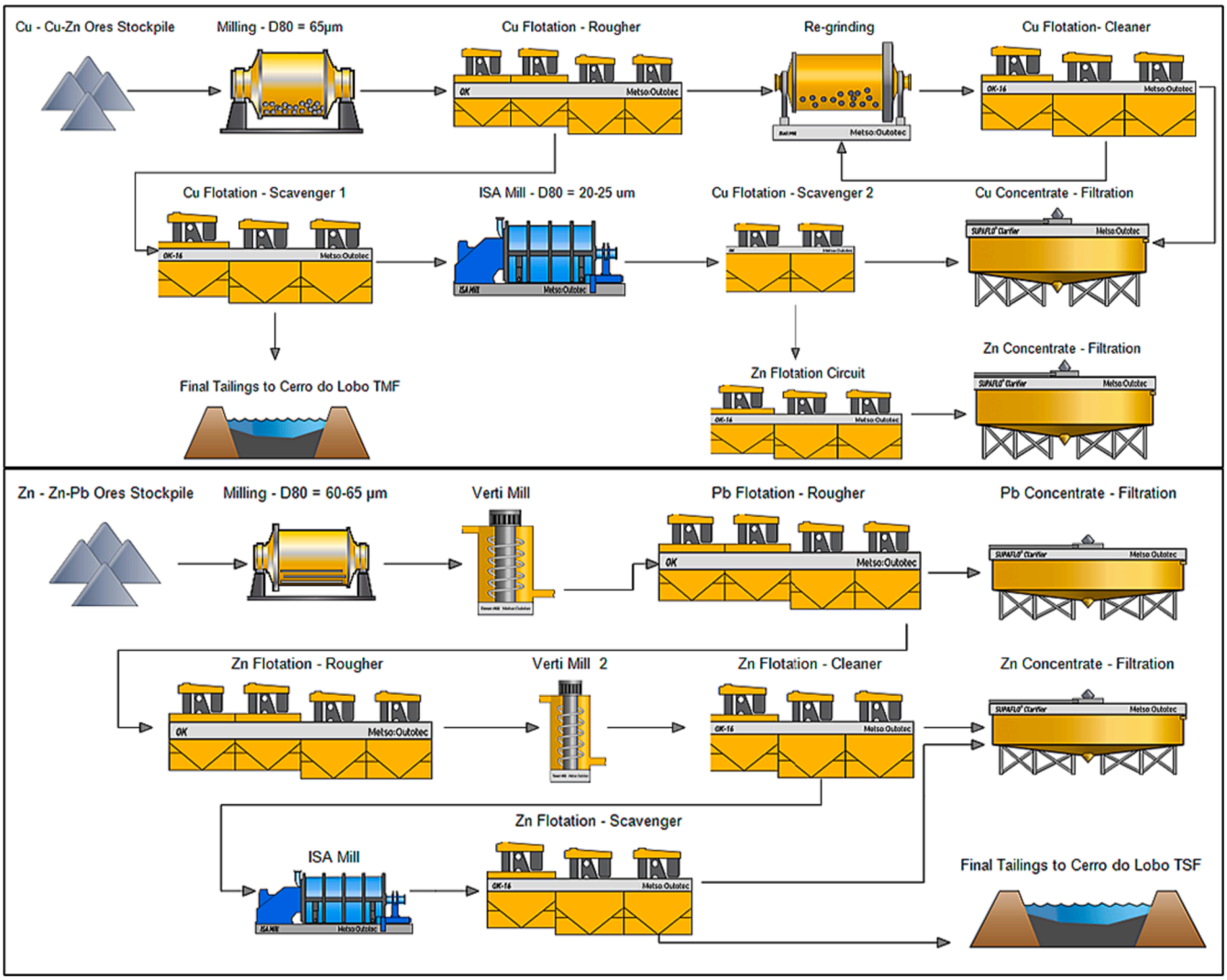

Fig. 1. Overall beneficiation scheme process for Copper processing (upper image) and Zinc-Lead processing plant (bottom image) at Neves Corvo mine (General information taken from a visit to Neves Corvo - February 2020).

largest product stream generated in minerals processing operations. The most common destination of the tailings is deposition in dams, also called tailings storage facilities (TSFs).

TSFs can have enormous dimensions, and the management and storage of such large volumes of material pose many challenges in terms of dam stability and immobilization of metal(loid)s and hazardous contaminants that present human health and environmental risks (Helser et al., 2022), particularly in sulfide-containing materials. In addition, considerable amounts of precious and base metals such as copper, lead, and zinc, which are economically valuable and have growing industrial demand, can remain in the tailings, turning them into potential sources of secondary raw materials.

The reprocessing of tailings has the potential to minimize the risks associated with their storage, and may also enable their use as sources of secondary raw materials. One potential route for tailings reprocessing is desulfurization. This refers to the separation of the sulfide minerals, generally the main source of acid generation and environmental pollution, from the tailings stream using a bulk sulfide flotation process (Demers, 2005; Nadeif et al., 2019; Skandrani et al., 2019; Benzaazoua et al., 2000; Bois et al., 2022). Desulfurization can have environmental and economic benefits when combined with the recovery of valuable minerals or metal(loid)s and the removal of hazardous contaminants. Furthermore, the sulfide-poor residue of the process may be used as a resource to manufacture new materials and products (e.g. construction materials such as geopolymers (Niu et al., 2021), ceramics (Simão et al., 2021; Veiga Simão et al., 2021), and inert or even active cement components (Martins et al., 2021).

Froth flotation is a highly efficient process for the concentration of sulfide minerals and can be the first step in tailings desulfurization. However, tailings contain a considerable amount of fine and ultrafine particles, which are, at present, a major challenge for the mineral processing industry. Therefore, this topic attracts much research attention (Demers, 2005; Gong et al., 2010; Wang and Liu, 2021; Sivamohan, 1990; Trahar and Warren, 1976; Somasundaran, 1978; Babel et al., 2018; Leistner et al., 2016).

The low flotation performance of fine and ultrafine particles is attributed to characteristics related to their small sizes, i.e. low inertial mass and high specific surface area (Demers, 2005; Wills and Finch, 2016). Their small size and low mass result in a low flotation rate because of a low probability of particle bubble collision and attachment and therefore an inefficient collection of particles, causing the loss of valuable hydrophobic mineral particles (Gong et al., 2010; Wills and Finch, 2016). The high surface area increases reagent consumption, enhances surface oxidation, and causes high solubility kinetics, which decreases selectivity (Demers, 2005). In addition, depletion in concentrate grade is caused by the mechanical and hydraulic entrainment of fine and ultrafine hydrophilic gangue particles (Gong et al., 2010; Wills and Finch, 2016; Wang et al., 2015).

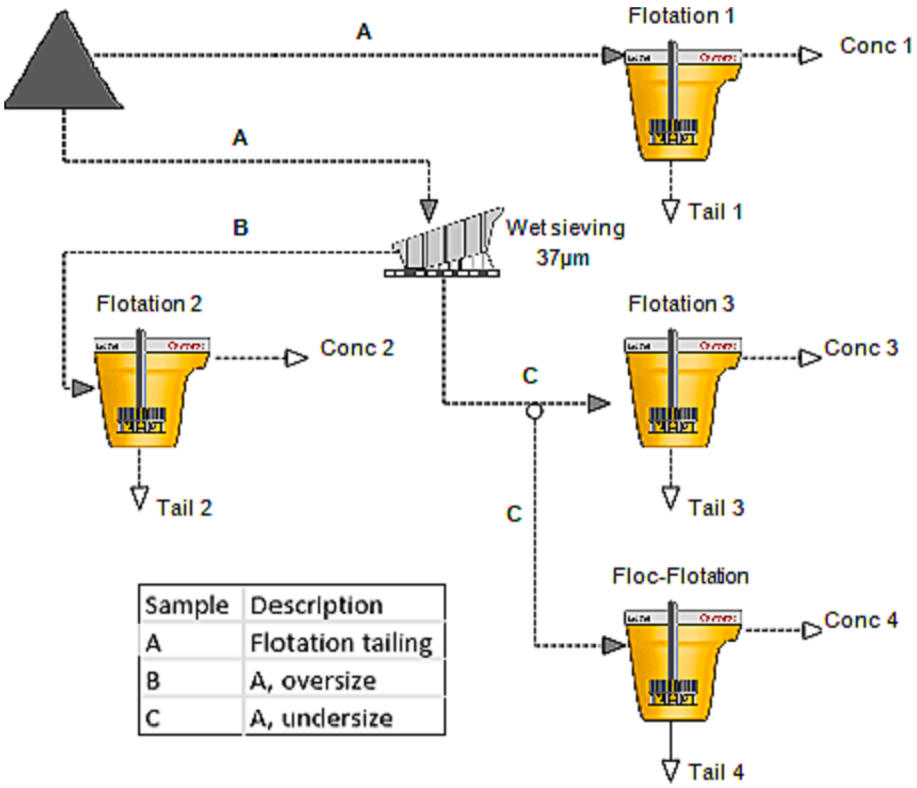

Fig. 2. Flotation routes studied. A: Neves Corvo tailing sample. B: oversize fraction from the wet sieving step. C: undersize fraction from the wet sieving step.

Overall, the flotation recovery of fine and ultrafine hydrophobic particles can be improved by decreasing bubble size and/or enlarging the particle size through agglomeration (Wang and Liu, 2021). The larger particles formed this way may, due to their greater size and inertia, increase the overall rate of collision and attachment to bubbles (Trahar and Warren, 1976). The particle sizes can be enlarged using inorganic depressants (Cao and Liu, 2006), polymer flocculants (Sivamohan, 1990; Wang and Liu, 2021; Mandre and Panigrahi, 1997; Mweene and Subramanian, 2018; Wang, 2013), hydrophobic interactions (Nogueira, 2019), and micro-organisms (Demers, 2005; Somasundaran et al., 1998). The flotation of the resulting agglomerates is termed floc flotation.

In this study, we assessed the recovery of sulfide minerals present in a sulfidic tailings material through a bulk direct flotation process. In addition, we evaluated the effect of particle agglomeration, using a polymer flocculant, in the recovery of the target elements.

The primary step to assess the recovery potential of the sulfide minerals was to quantify the abundance, nature, distribution, and occurrence of sulfide minerals in the tailing samples collected from the processing plant. By applying scanning electron microscopy (SEM)-based image analysis coupled to energy dispersive x-ray analysis (EDX) in combination with wet chemical assaying by inductively coupled plasma optical emission spectroscopy (ICP-OES), as well as laser diffraction, and mass balance, it was possible to quantitatively characterize different chemical, mineralogical, and microstructural parameters (such as grade, modal mineralogy, mineral association, mineral liberation, grain and particle sizes, and other process-related properties) and identify a suitable process route for sulfide recovery through flotation.

2. Materials and methods

2.1. Neves Corvo mine site description

The Neves Corvo mine is situated in the Portuguese sector of the well-known Iberian Pyrite Belt (IPB), which has distinctive ore occurrences and mineralogical characteristics. The IPB comprises more than 85 known ore deposits, mostly occurring as massive sulfide ores (Relvas, 2000). The Neves Corvo mine has been classified as a volcanogenic massive sulfide deposit with distinctively high grades of copper, zinc, and tin compared to other deposits. By far the most common sulfide mineral present at Neves Corvo is pyrite, frequently associated with sphalerite, galena, chalcopyrite, and arsenopyrite, and accompanied by non-sulfide gangue minerals such as quartz, chlorite, muscovite, and carbonates (Gaspar, 2002; Relvas et al., 2006).

Since commencing mining operations in 1988, at least seven ore bodies have been found/exploited, producing copper (1988-present), tin (1991–2000), zinc, and lead (from 2006), and other minor by-products (Relvas et al., 2002; Escobar et al., 2021). Currently, the Neves Corvo mine has copper and zinc processing units. The first has a maximum capacity of 2.6 Mt/a and processes copper and copper-zinc ores, while the second one has also a maximum capacity of 2.6 Mt/a (expansion completed in February 2022) and processes zinc and zinc-lead ores (Escobar et al., 2021).

The beneficiation process comprises, in addition to the primary grinding processes, two main stages: flotation and re-grinding. The overall beneficiation process scheme is shown in Fig. 1 for both processing plants. Tailings from the rougher circuit of the flotation process are re-ground in an ISAmill where particle size is reduced from 65 µm to 25 µm (average D80) and sent back to a scavenger flotation circuit to increase metal recovery from finer particles (Oliveira, 2019).

The copper processing plant is fed with ores with grades around 1.5 % - 3.5 % (w/w) Cu while the zinc processing plant is fed with ores with grades between 7.5 % and 9 % (w/w) Zn and 1.5 % - 2.5 % (w/w) Pb. Final concentrates produced by both processing plants vary between 46 % and 48 % (w/w) Zn, 22 % - 23 % (w/w) Cu, and 25 % - 35 % (w/w) Pb, with recoveries of 84 % and 88 % for Zn and Cu, respectively. The tailings from both processing facilities are combined and piped to the Cerro do Lobo Tailings Management Facility (TMF).

Table 1
Samples investigated via mineral liberation analysis (MLA).

Sample	Description
A	Neves Corvo tailing sample
B	Oversize from sieving of A
C	Undersize from sieving of A
Conc 2	SIBX 50 g/t, 0 min – 5 min flotation
Tail 2	SIBX 50 g/t, 0 min – 5 min flotation
Conc 3	SIBX 100 g/t, 0 min – 10 min flotation
Tail 3	SIBX 100 g/t, 0 min – 10 min flotation
Conc 4 -A	SIBX 100 g/t, SFN100 50 g/t, 0 min – 5 min flotation
Conc 4 -B	SIBX 100 g/t, SFN100 50 g/t, 5 min – 10 min flotation
Tail 4	SIBX 100 g/t, SFN100 50 g/t, 0 min – 10 min flotation

2.2. Flotation routes

Bench-scale flotation tests were performed using Neves Corvo tailings (A) aiming at a collective recovery of the sulfide minerals in a rougher flotation. In a later stage, the sample was divided into two fractions through wet sieving, using a 37 μm screen, and the flotation of the over- and undersize fractions, namely B and C, in different routes was evaluated. For the processing of sample C, the use of floc flotation was also assessed. The flowchart of the four flotation approaches used in this work is presented in Fig. 2.

2.3. Samples and reagents

The Neves Corvo tailings samples are formed by the mixed tailings streams coming from the copper and zinc processing plants before disposal at the Cerro do Lobo tailings pond. The slurry contains gangue minerals and low residual quantities of valuable metals that were not recovered during the beneficiation process. The major gangue minerals in the tailings comprise pyrite, quartz, and phyllosilicates, while the main valuable minerals include sphalerite, galena, and chalcopyrite. Correspondingly, the major chemical components of the tailings are Fe (~26 % (w/w)), SiO_2 (~33 % (w/w)), and sulfur (24 % – 28 % (w/w)), with minor amounts of Zn (0.7 % – 1.3 % (w/w)), Pb (0.3 % – 0.7 % (w/w)), and Cu (0.3 % – 0.6 % (w/w)) (Escobar et al., 2021).

A sampling campaign was executed in April 2019 by SOMINCOR, which involved the collection of buckets of 25 kg slurry with 60 % - 66 % of solids. The sample was stored and transported underwater to prevent oxidation. Following the removal of the supernatant water layer, the sample was dried at 40 °C, deagglomerated, homogenized, and split using a rotary splitter. The sub-samples were stored in plastic bags under vacuum and refrigerated (4 °C) to prevent oxidation.

A wet-sieving step was performed on a representative split of the Neves Corvo tailings sample (A), using a W56 Linear Motion Screen (Derrick Corporation) equipped with a wire screen panel of 400 US mesh (37 μm). The device is equipped with wash water spray bars with multiple nozzle styles that enhance the removal of fines from oversize fractions. To increase the efficiency of the sieving step, the moisture content of the sample was increased to 70 % beforehand, and the oversize fraction was sieved twice. The products of the sieving were stored under water to prevent oxidation.

2.4. Characterization

The elemental composition of samples A, B, C, and of the concentrates and tailings from flotation experiments was analyzed using ICP-OES 5100 (Agilent Technologies, USA). Melt digestion (Li2B4O7-melt leached with HCl) was employed to analyze Al, Mg, and Si. Microwave-heated HCl/HNO_3 digestion using a TurboWAVE® autoclave (MLS-MWS Laboratory solutions, Switzerland) was used to analyze As, Ca, Co, Cr, Cu, Fe, Mn, Pb, and Zn. To analyze sulfur, the samples were mixed with MgO/Na_2CO_3, ignited for 4 h at 815 °C, and leached with water.

Granulochemical analysis was performed on a representative subsample of A. First, the sample underwent a wet sieving step using an electromagnetic sieve shaker (EML 200 digital T, Harver, Germany) with nine screen size apertures (150 μm, 100 μm, 90 μm, 80 μm, 63 μm, 40 μm, 32 μm, 25 μm, 20 μm). Afterward, a representative sample of the fraction −20 μm was further sieved with three additional screen size apertures (15 μm, 10 μm, and 5 μm) using an EMS 755 electromagnetic sieve shaker (TOPAS, Germany) and an ultrasonic processor UP 200S (Hielscher, Germany). The mass of each fraction was dried, weighed, and prepared for chemical analysis via ICP-OES.

The particle size distributions (PSD) of samples A, B, and C were measured via laser diffraction using a Sympatec Helos/KR with a Quixel disperser (Sympatec GmbH, Germany). The sieving efficiency was calculated according to (Gupta et al., 2006).

Mineral Liberation Analysis (MLA), a scanning electron microscopy (SEM) and energy dispersive x-ray analysis (EDX)-based automated image analysis method was used to investigate the mineral phases present in the samples (Table 1) and provide quantitative mineralogical and microstructural data based on the back-scattered electron (BSE) intensity and X-ray emission spectra of the minerals (Gu, 2003). Phases with higher average atomic numbers have a higher BSE intensity and are brighter in the grey-scale images compared to phases with lower average atomic numbers. The particle-specific mineralogy data from MLA measurements can be used to develop a detailed understanding of the interaction between particle properties and process outcomes (Pereira et al., 2021; Pereira et al., 2021). In the present study, MLA was used to provide quantitative mineralogical and textural data which helped to understand the processes occurring during flotation and assess how the flowsheet could be improved.

Analyses were performed at the Helmholtz Institute Freiberg for Resource Technology (HIF) on an FEI Quanta 650F field emission SEM (FE-SEM) equipped with two Bruker Quantax X-Flash 5030 energy-dispersive X-ray (EDX) detectors and the MLA software suite version 3.1. In preparation for analysis with MLA, 2 g of each sample was mixed with graphite powder and embedded in epoxy resin (25 mm). To reduce the effects of gravity settling of particles in the epoxy resin due to different particle sizes and densities, the original mounts were cut vertically, rotated by 90°, re-embedded into epoxy resin, and polished to obtain grain mounts of 30 mm. The grain mounts were subsequently carbon-coated to prevent charging effects during the measurements (Heinig et al., 2015).

The samples were analyzed with the GXMAP measurement mode, where particles and mineral grains are segmented based on their BSE intensity, and X-ray spectra are collected in a grid-pattern to characterize the identified phases (Gu, 2003; Fandrich et al., 2007). The MLA was operated at 25 kV (acceleration voltage), 10 nA (probe current), 4.78 μm spot size, and horizontal frame width of 500 μm (750 μm for samples C). Minerals/phases present are classified by matching the measured X-ray spectra to a mineral reference list. Due to the fine-grained nature of the tailings samples, several mixed spectra were added to the mineral reference list at ratios of 2:1 and 1:2, to enable the classification of fine sulfide mineral grains (Bachmann et al., 2017; Kern et al., 2018; Blannin et al., 2021). The minimum spectral matching threshold for classification was set at 80 %, and the classified data were processed with several software scripts to assign measurements with mixed spectra to the correct phases.

2.5. Froth flotation

Sample A was stored under vacuum and refrigerated to avoid oxidation. Samples B and C were stored underwater, with around 40 % solids. Before the flotation experiments, the suspensions of samples B and C were homogenized using an overhead stirrer (IKA, RW 28 digital) at 1000 min^{-1} for 5 min. While stirring, a representative sample was taken using a 0.5 l glass container. The batch flotation tests were conducted in a Denver-type flotation machine (own development) using a 0.3 l capacity cell.

Table 2
Chemical assays of samples A, B, and C as measured by ICP-OES.[a]

Element	Unit	A	B	C
		Avg.	Avg.	Avg.
Al	%	3.03	2.91	3.23
As	%	0.44	0.31	0.52
Ca	mg/kg	5505	3103	2329
Cd	mg/kg	7	36	17
Co	mg/kg	192	134	184
Cr	mg/kg	37	96	54
Cu	%	0.36	0.35	0.36
Fe	%	27.14	24.24	28.82
Mg	mg/kg	9004	9935	8970
Mn	mg/kg	673	668	622
Pb	%	0.35	0.30	0.35
S	%	25.85	21.77	26.33
Si	%	13	17	12
Zn	%	0.97	1.46	0.72

[a] Tested in duplicate and reported data are mean values.

Three flotation strategies were tested in this study, as illustrated in Fig. 1:

a. No sieving before flotation (Flotation 1);
b. One sieving step before flotation and two conventional flotation routes for the under- and oversize products (Flotation 2 and 3);
c. Floc flotation for sample C.

Copper sulfate (Sigma-Aldrich) was used as a sphalerite (Zn) activator, sodium isobutyl xanthate (SIBX, Yantai Billion Thai Chemical Co. LTD - production specification of BioSO4 Oy) was used as the promoter (collector) of sulfide minerals, methyl isobutyl carbinol (MIBC, Sigma-Aldrich) was used as a frother, and sulfuric acid (Honeywell, Fluka) and sodium hydroxide (Windaus-Labortechnik) were used for pH adjustment when needed. In the tests using flocculation, the high molecular weight, non-ionic polyacrylamide Superfloc N100 (SFN100) (supplied by Kemira) was used. A 0.1 % (w/v) stock solution was prepared daily.

Preliminary flotation tests were performed with sample A (not presented here), and the following conditions gave the best results in terms of S grade and recovery: pH 6 ± 0.2, 300 g/t (dry basis) copper sulfate, 100 g/t (dry basis) SIBX, and 100 g/t (dry basis) MIBC. In the case of floc flotation, SFN100 was added to the flotation cell before the addition of SIBX, and SFN100 dosages of 10 g/t, 50 g/t, and 100 g/t were tested. The experiments were performed with deionized water and 25 % solids. The reagents were conditioned in the flotation cell using an impeller speed of 1400 min^{-1} for 5 min. Flotation was conducted with the same impeller speed and airflow of 0.6 l/min.

After each flotation experiment, the mass of the products was measured before and after drying to determine the dry mass recovery and the water recovery. Drying was performed in an oven under natural convection for 24 h at 40 °C, followed by the preparation of representative dry samples for characterization. The flotation recoveries and the enrichment were then calculated. Each flotation test was performed at least twice. The data presented in Figs. 9–12 are the mean values and the standard deviation (SD).

3. Results

3.1. Sample characterization

3.1.1. Particle size distribution of feed samples

Results from laser diffraction analyses showed that A has a D20, D50, and D80 of 4 μm, 16 μm, and 66 μm, respectively. Other research works on the Neves Corvo extractive mine residues found a similar particle size distribution (Escobar et al., 2021; Schueler et al., 2021). After the wet sieving step, samples B and C corresponded, respectively, to c. 33 % and 67 % of sample A. Sample B has a D20, D50, and D80 of 44 μm, 81 μm, and 139 μm, respectively, while C has a D20, D50, and D80 of 2 μm, 6 μm, and 16 μm, respectively. The efficiency of the screen was determined to be 89 % (Gupta et al., 2006). The detailed results from the laser diffraction analyses of samples A, B, and C can be found in Appendix A, Figs. A.1–A.3.

3.1.2. Chemical assays of feed samples

As anticipated from the mineralogy of the tailings (Escobar et al., 2021; Schueler et al., 2021; Opara et al., 2022; Kamariah et al., 2022), Fe, S, and Si are the most abundant elements in the three samples, as shown in Table 2. Valuable metals (Zn, Cu, and Pb) and toxic metal(loid)s (As, Cd) are also present at low concentrations. Compared to the original sample (A), the oversize fraction (B) contains higher Si and Zn grades, indicating that these elements are more abundant in the coarser fractions. In turn, the undersized fraction has a chemical composition more similar to A, which could be expected since it represents the larger proportion of the original sample mass.

Results from the granulochemical analysis of sample A (Fig. 3) identified higher grades of Si and Zn in the coarser fractions (+40 μm), and slightly higher Fe and S grades in the finer fractions (-40 μm). The detailed elemental distribution can be found in Appendix B, Table B.1. These findings corroborate the chemical assays of the over- and undersize fractions.

Table 3 presents the retained percentages (w/w) of Cu, Pb, S, and Zn in the three main size classes relevant to this study (0 μm – 5 μm, 5

Table 3
Cumulative percentages of Cu, Pb, S, and Zn from the granulochemical analysis, as measured by ICP-OES.

Screen size	Cu	Pb	S	Zn
μm	(%)	(%)	(%)	(%)
40–200	39.6	35.3	37.6	64.9
5–40	20.3	12.2	33.7	14.1
0–5	40.1	52.5	28.7	21.0

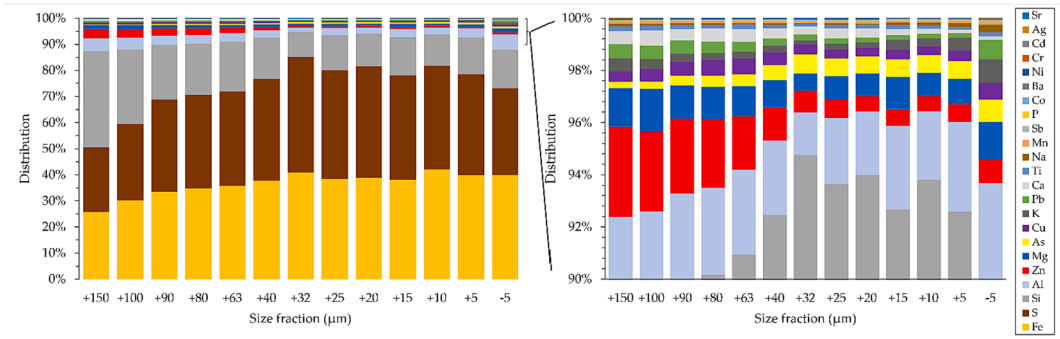

Fig. 3. Chemical assays of the granulochemical analysis of Neves Corvo tailings (sample A), as measured by ICP-OES.

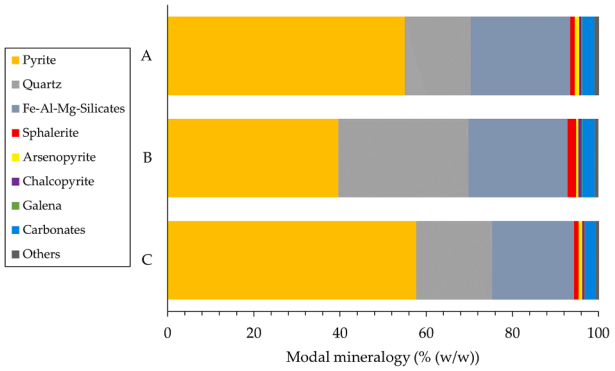

Fig. 4. Modal mineralogy (% (w/w)) of the feed streams, obtained with MLA.

Table 4
Deportment of As, Cu, Fe, Pb, S, and Zn (in % (w/w)) in the Neves Corvo tailings, according to MLA.

Mineral grouping	As	Cu	Fe	Pb	S	Zn
Pyrite			85.1		97.2	
Silicates			10.1			
Sphalerite			0.1		1.2	100.0
Chalcopyrite		62.4	0.5		0.5	
Galena				99.9	0.1	
Arsenopyrite	93.3		1.1		0.6	
Other sulfides		1.3				
Carbonates			3.0			
Sulfosalts	6.7	36.3		0.1	0.2	
Others			0.1		0.1	
Total	100.0	100.0	100.0	100.0	100.0	100.0

μm – 40 μm, and 40 μm – 200 μm). Note that 52 % Pb and 40 % Cu contained in the Neves Corvo tailings sample are present in ultrafine particles smaller than 5 μm, and circa 65 % of the Zn is present in the coarser fraction.

3.1.3. Mineralogical analyses

MLA was used to define and quantify the mineral phases present in the samples, the association and liberation of the minerals, as well as their grain and particle size distributions. Based on the results of MLA, 45 individual mineral species were identified in the tailings and were classed into 9 groups (Appendix C - Table C.1). The modal mineralogy of samples A, B, and C is given in Fig. 4 for the 9 mineral groupings.

As expected from the geology and mineralogy of the Neves Corvo ore and previous work on the same tailings material (Relvas et al., 2006; Escobar et al., 2021; Gaspar and Pinto, 1991; Frenzel et al., 2019), the mineralogy of the tailings is dominated by pyrite, as well as silicates, comprised mainly of quartz, feldspars, and chlorites. Other sulfide minerals hosting the metals of interest are present in lower contents, as well as carbonates. The mineralogy of the B and C samples are similar to that of A, but the minerals occur in different proportions.

Sulfide minerals are the dominant hosts of As, Cu, Fe, Pb, S, and Zn in the Neves Corvo tailings. The elemental distribution, as calculated from the modal mineralogy and the standard mineral compositions, is given in Table 4. Cu is present primarily in chalcopyrite and sulfosalts (tennantite, tetrahedrite), and in minor amounts in other Cu sulfides. Sphalerite and galena are the main hosts of Zn and Pb, respectively, while As mainly occurs in arsenopyrite, with minor amounts hosted by sulfosalts (tennantite and enargite). Pyrite is the most abundant sulfide mineral and accounts for the majority of Fe (85.1 % (w/w)) and S (97.2 % (w/w)). These results corroborate the findings of Kamariah and coworkers on the Neves Corvo tailings sample (Kamariah et al., 2022).

Cu, S, and Zn MLA back-calculated assays were in good agreement with the chemical assay for the samples, within analytical uncertainties, while MLA underestimated the Pb content in all studied process samples, as shown in Fig. 5.

Fig. 6 shows BSE images and false color images of the common association between the sulfide minerals in the Neves Corvo tailings sample, with galena often locked in pyrite as finely disseminated grains, not all of which are detected by the MLA, as indicated with the blue arrows. This means that MLA is most likely underestimating the ultrafine-locked galena particles.

In this work, we consider fully liberated particles as those with a free surface of 80 % or more, partially liberated particles are those with 20 % - 80 % of free surface, and locked particles are those with 0 % - 20 % of free surface. As can be seen in Fig. 7, pyrite has a large proportion of liberated particles: 78.9 % A, 70.6 % B, and 85.2 % C. A significant proportion of the Cu-, Zn-, and Pb-sulfide minerals in the three samples, on the other hand, are not (or only partially) liberated (Fig. 7) and are mostly associated with pyrite (Fig. 8). The liberation distributions used in this study are calculated based on the two-dimensional (2D) sectional analysis. It is known that 2D analysis somewhat overestimates the degree of liberation (Gaudin, 1939).

The mineral association results from MLA are given in Fig. 8. The main mineral interlocked with sphalerite, chalcopyrite, and galena is pyrite. The proportion of locked particles increases with particle size, i.e. liberation by free surface of the three minerals decreases in sample B.

3.1.4. Froth flotation

In this work, a collective rougher flotation of the sulfide minerals was performed. As detailed in Section 2.5, three flotation approaches were used: 1) flotation of the material as received (sample A, producing Conc 1 and Tail 1); 2) classification of the material into two particle size ranges before flotation (sample B, oversize fraction, producing Conc 2 and Tail 2, and sample C, undersize fraction, producing Conc 3 and Tail 3), and 3) floc flotation of the undersize particles (producing Conc 4 and Tail 4). Eight overflow products were collected to study the kinetics of samples A and C with the following collection times: 0.5 min, 1 min, 2 min, 4 min, 6 min, 8 min, 13 min, and 16 min. Seven overflow products were collected to study the kinetics of sample B with the following collection times: 0.5 min, 1 min, 2 min, 4 min, 6 min, 8 min, and 10 min.

The three approaches resulted in distinct separation efficiencies. The recovery versus grade curves for S, Cu, Zn, and Pb in the concentrates (Conc 1–3) are shown in Figs. 9–12a, respectively. The grade versus time curves for S, Cu, Zn, and Pb in the tailings (Tail 1–3) are presented in Figs. 9–12b, respectively.

Overall, the grade/recovery curves for all elements show that the Conc 2 curve always lies markedly ahead of those obtained for Conc 1 and 3 (Figs. 9–12a). This could be expected considering that coarser particles present faster flotation kinetics. The first-order rate constants for Cu, Pb, S, and Zn flotation with samples A, B, and C are presented in Appendix D – Table D.1.

In particular, for S recovery, the curves of Conc 1 and 3 were quite similar, regardless of using Neves Corvo tailings as received or the undersize fraction (Fig. 9a). After 4 min of flotation, for instance, Conc 2 recovers circa 95 % of S (±0.6 %), while in Conc 1 and 3 the S recovery is 74 % (±0.1 %) and 77 % (±0.9 %), respectively. In terms of S grade, the three concentrates present similar results for the same flotation times. Tails 1 and 3 present 4.20 % S (±0.33 %) and 3.38 % S (±0.49 %), respectively, after 16 min of flotation (Fig. 9b). Tail 2 has 2.13 % S (±0.28 %), after 4 min of flotation and it reaches as low as 1.56 % (±0.27 %) within 10 min of flotation.

Conc 2 and 3 have, respectively, slightly higher and lower Cu grades as compared to Conc 1 (Fig. 10a). Tails 1 and 3 present 0.11 % Cu (±0.01 %) and 0.10 % Cu (±0.01 %), respectively, after 16 min of flotation (Fig. 10b). Tail 2 has 0.09 % Cu (±0.01 %), after 4 min of flotation and it reaches as low as 0.07 % (±0.01 %) within 10 min of flotation.

Fig. 11a displays a clearly superior separation efficiency for Zn from Conc 2 and the differences between the three concentrates are more evident than for S and Cu. The grade of Zn in the feed samples (grades at

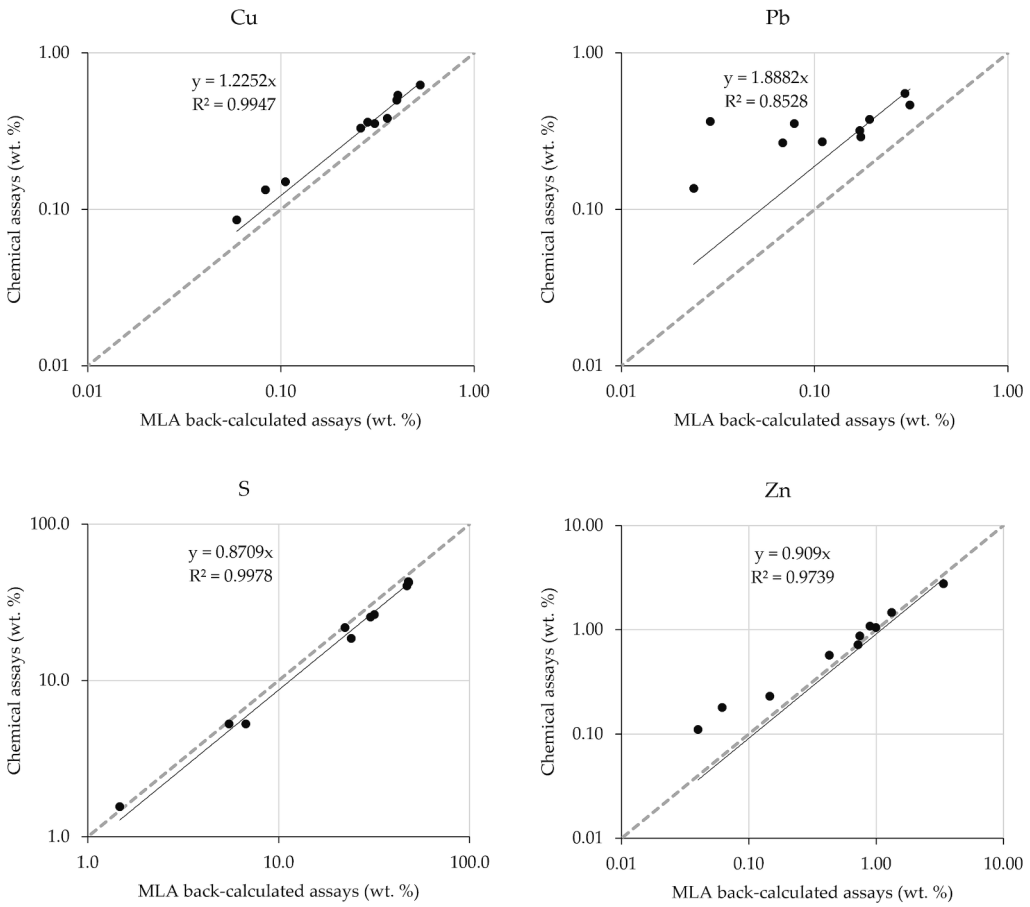

Fig. 5. Comparison between the results of mineral liberation analysis (MLA) back calculated assays and chemical assays. The line patterns (solid line, dashed line) represent the best fit and the 1:1 line, respectively.

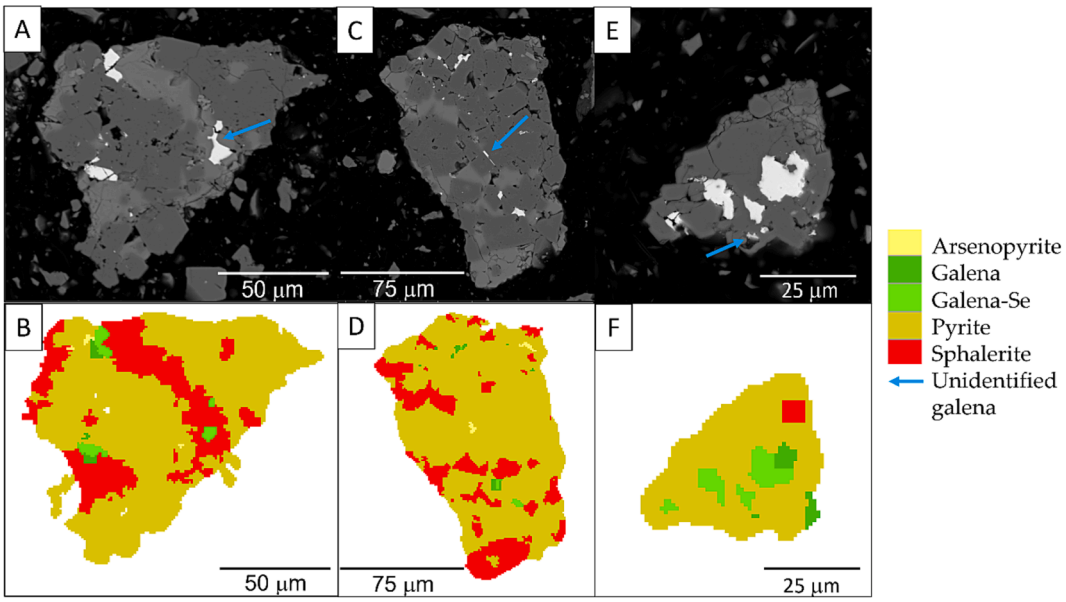

Fig. 6. BSE images (A, C, E) and false color images from MLA (B, D, F) of associations of pyrite with other sulfide minerals in Neves Corvo tailings sample. The common association of pyrite grains with arsenopyrite, galena, galena-Se, and sphalerite is shown in A-B and C-D, and with galena, galena-Se, and sphalerite in E-F.

time 0 min in Fig. 11b) may explain this effect.

Fig. 12a shows that the Pb grade in the concentrate (Conc 3) of the fine particle flotation remains lower than the Pb grade in the feed sample (0.35% Pb) throughout the entire duration of flotation. Conversely, Fig. 12b demonstrates that in tailings (Tail 3), the Pb content reaches 0.41% (±0.03) at 6 min of flotation, indicating that galena is remaining in the tailings. This is most likely due to both the reduced entrainment caused by heavier particles of lead-bearing phases at similar sizes of

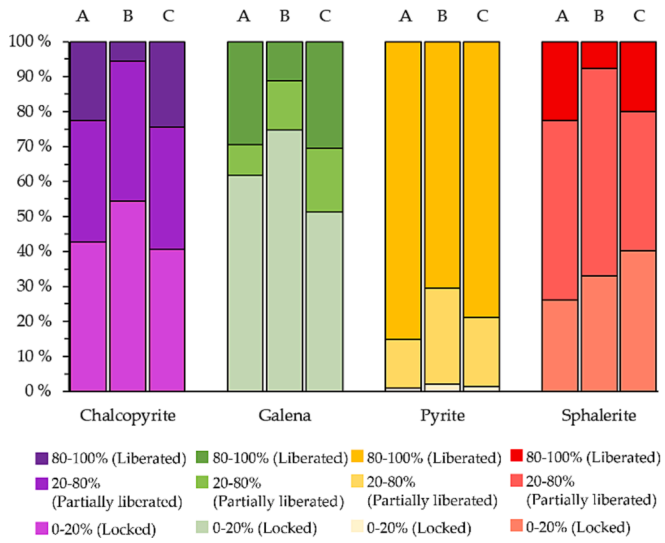

Fig. 7. The free surface of particles of chalcopyrite, galena, pyrite, and sphalerite in A: Neves Corvo tailing sample, B: oversize wet sieving, and C: undersize wet sieving.

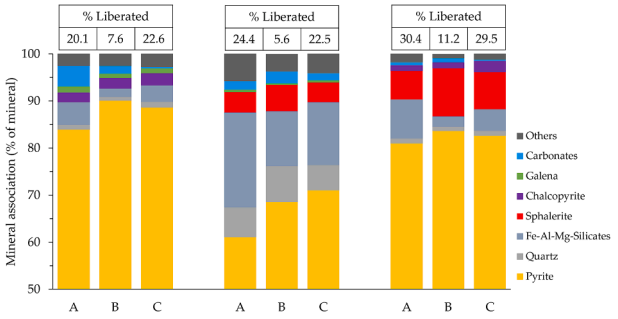

Fig. 8. Sphalerite (left), chalcopyrite (center), and galena (right) association with other minerals A: Neves Corvo tailing sample, B: oversize wet sieving, and C: undersize wet sieving $\left(Mineral\ \ association = \frac{\%\ \ mineral\ \ surface}{100-\%\ \ free\ \ surface} * 100\right)$

other entrained material, as well as slower "true flotation" of lead-bearing sulfides. A summary of the results from the characterization of the flotation products is presented in Appendix E - Tables E.1–E.3.

MLA and ICP-OES were used to quantify the mineral phases and the chemical assays in Conc 2 and Tail 2 (obtained using 50 g/t SIBX and 5 min of flotation) and Conc 3 and Tail 3 (obtained using 100 g/t SIBX and 10 min of flotation) and the results are presented in Fig. 13. It is observed that regardless of the particle size of the feed sample, Conc 2 and Conc 3 achieved high pyrite grades (84.5% and 87.7%, respectively). Nevertheless, the flotation of B achieves the highest Zn, Cu, and Pb grades in the concentrate and produces the cleanest tailings, using half of the collector dosage and within a shorter time. This can be explained by the fact that the finer particles in sample C have a specific surface area about 8 times larger than the coarse particles in sample B, therefore more collector is needed to create a monolayer on the surface of the particles in sample C.

Fig. 14 shows that the results of the modal mineralogy obtained from the analysis of samples B and C and the back-calculated results obtained from the modal mineralogy of the flotation products are very similar. The differences are within an error that is acceptable for MLA measurements. In addition, it is observed that with a lower mass pull, Conc 2 recovers markedly more pyrite than Conc 3.

It is known that the flotation of the sulfide minerals would become more efficient if the recovery of ultrafine sulfide-bearing particles was improved. Therefore, in this research, a non-ionic, high molecular weight polyacrylamide, SFN100, was used to increase the dimensions of the particles before flotation (floc flotation).

Preliminary flocculation tests were performed using SFN100 on sample A suspensions. The flocs were observed using a microscope and big bright particles (most probably silicate minerals) were visualized entrapped in the flocs (Fig. 15). In physical terms, the addition of polymer to a distribution of particle sizes causes the formation of randomly shaped, open floc structures into which unwanted material can easily become trapped (Wightman et al., 2000). It was observed that a considerable proportion of the particles present was already a suitable size for conventional flotation, with no need for flocculation. For that reason, the floc-flotation approach was evaluated using only sample C. The influence of the flocculant dosage on the mass and gangue recovery and the recovery and grade of Cu, Pb, Zn, and S was evaluated, and the results are summarized in Fig. 16.

On one hand, it is noticeable that the mass and gangue recovery increase with the addition of SFN100. On the other hand, the separation efficiency is dramatically improved for Pb. Conversely, flocculation had

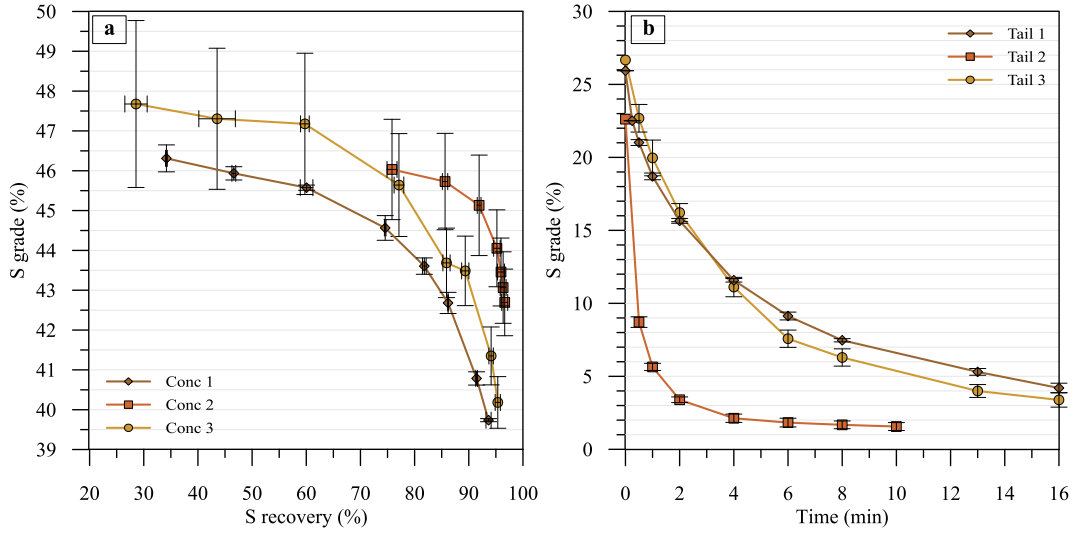

Fig. 9. S grade and recovery in the (**a**) concentrates (Conc 1–3) and (**b**) grade versus time in the tailings (Tail 1–3). The experiments were performed using 300 g/t CuSO4, 100 g/t SIBX, 100 g/t MIBC, pH 6, and 25 % solids.

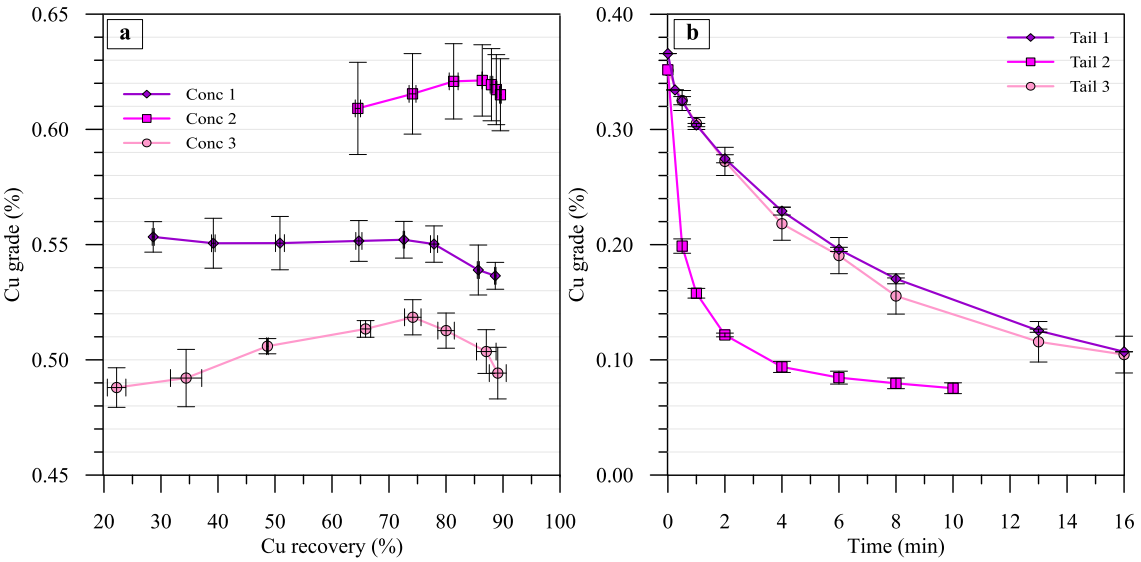

Fig. 10. Cu (**a**) recovery versus grade in the concentrates (Conc 1–3) and (**b**) grade versus time in the tailings (Tail 1–3). The experiments were performed using 300 g/t CuSO4, 100 g/t SIBX, 100 g/t MIBC, pH 6, and 25% solids.

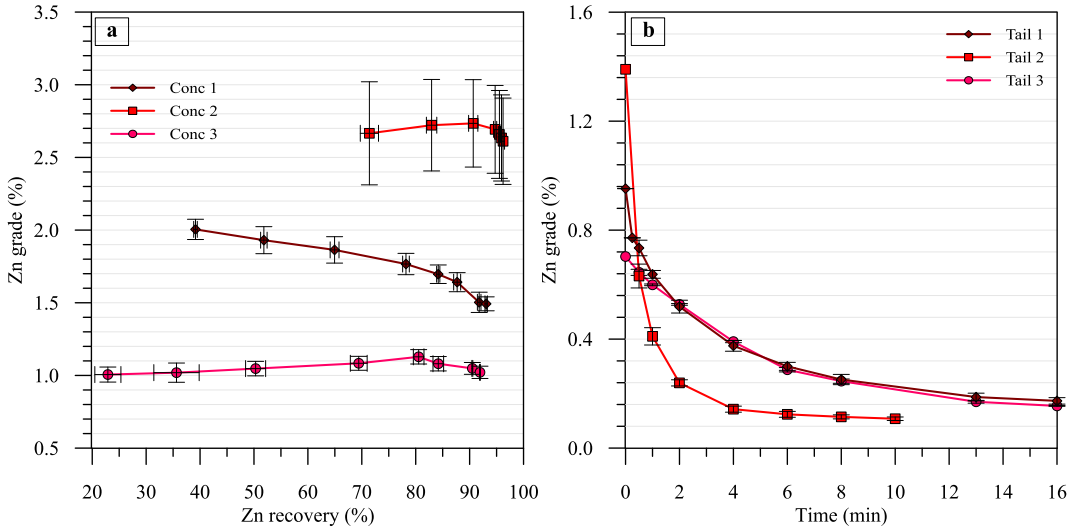

Fig. 11. Zn (**a**) recovery versus grade in the concentrates (Conc 1–3) and (**b**) grade versus time in the tailings (Tail 1–3). The experiments were performed using 300 g/t CuSO4, 100 g/t SIBX, 100 g/t MIBC, pH 6, and 25% solids.

no effect on Cu separation efficiency, but an inverse effect on Zn and S. Therefore, the improvement in the flotation of Pb is likely to be explained solely due to froth/entrainment effects caused by the flocculant addition, and thus there is no evidence for improved selectivity through "true flotation".

Product samples from the floc flotation were investigated via MLA and ICP-OES. A comparison between the floc flotation and the conventional flotation products for 10 min flotation time is presented in Figs. 17 and 18. The experiments were performed using the same parameters, aside from the addition of 50 g/t SFN100 before the collector in the floc flotation.

It can be observed that the addition of flocculant decreased the pyrite grade in Conc 4 from 87.7% to 80.5% and increased the Pb content from 0.29% to 0.40%, while Tail 4 contains lower pyrite, Zn, Cu, and Pb contents (Fig. 17). The flocculation increased the mass pull in the concentrate from 56.8% to 64.8% (Fig. 18) leading to slightly higher recoveries of sulfides in Conc 4 and a noticeable increase in the entrainment of quartz and Fe-Al-Mg-Silicates. These results corroborate the findings that flotation becomes less selective as flocculant is added.

Samples from the initial (Conc 4-A) and the final (Conc 4-B) 5 min of floc flotation were analyzed via MLA and ICP-OES to investigate the fractional recoveries in the concentrate and the results are presented in Fig. 19. It is noticed that the biggest mass pull is obtained in the first 5 min of flotation, therefore in Conc 4-B, the contribution in the pyrite recovery is markedly smaller. On the other hand, the Pb grade in Conc-B is higher than in Conc 4-A. Additionally, it can be observed that floc flotation has a faster flotation rate, with Conc 4-A reaching a mass pull of 56.8% in 5 min of flotation, which was only obtained in Conc 3 after 10 min.

Fig. 20 presents the modal mineralogy of the products from the floc flotation and the conventional flotation for the same mass pull. It can be observed that the addition of flocculant decreased the pyrite and increased the Fe-Al-Mg-Silicates content in the concentrate.

Additional mineralogical parameters, such as mineral liberation, were studied for the flotation products to provide valuable information for the beneficiation stages. Fig. 21 presents the liberation by free

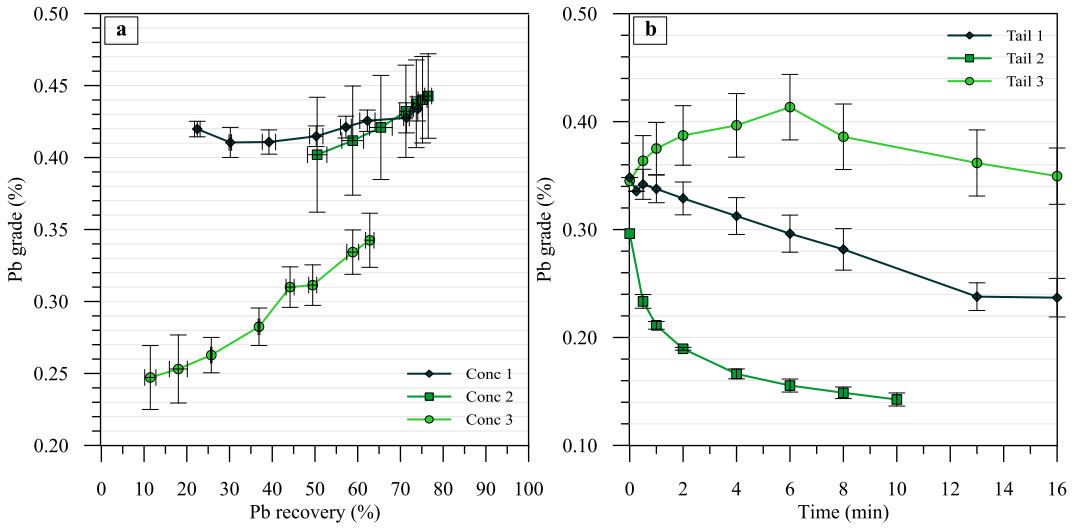

Fig. 12. Pb (**a**) recovery versus grade in the concentrates (Conc 1–3) and (**b**) grade versus time in the tailings (Tail 1–3). The experiments were performed using 300 g/t CuSO4, 100 g/t SIBX, 100 g/t MIBC, pH 6, and 25% solids.

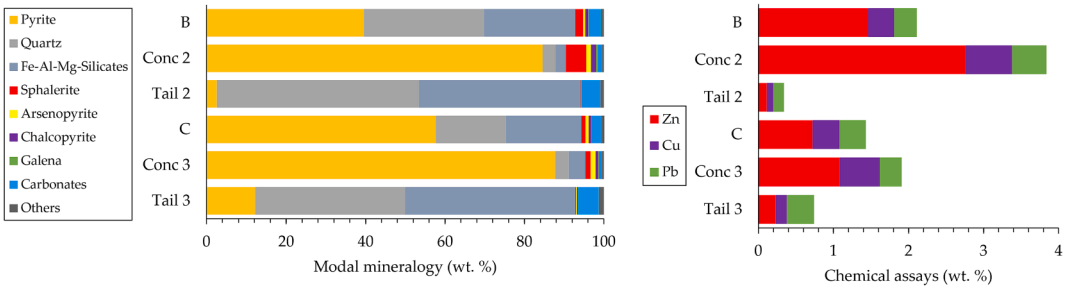

Fig. 13. Modal mineralogy (wt. %) and Zn, Cu, and Pb assays of feed (B and C), concentrate (Conc 2–3), and tailings (Tail 2–3) samples, obtained, respectively, with MLA and ICP-OES. Conc 2 and Tail 2 (obtained using 50 g/t SIBX and 5 min of flotation) and Conc 3 and Tail 3 (obtained using 100 g/t SIBX and 10 min of flotation).

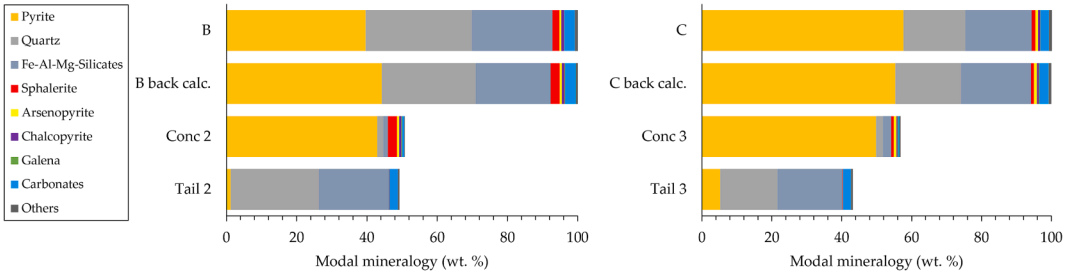

Fig. 14. Modal mineralogy (wt. %) of feed (A and B), concentrate (Conc 2–3), and tailings (Tail 2–3) samples, obtained with MLA. B and C back calc. are the modal mineralogy of the feed samples calculated from the modal mineralogy of the flotation products. The modal mineralogy of Conc 2, Tail 2, Conc 3, and Tail 3 does not sum to 100%, since it illustrates the relative mass flow of the different minerals.

surface of the target sulfides in Conc 4-A, Conc 4-B, and Tail 4. It indicates that highly liberated pyrite particles were well recovered throughout the experiment, which could be expected knowing that pyrite particles present in the Neves Corvo sample are mostly liberated (Fig. 7). In turn, in the first 5 min of flotation, the concentrate mostly consisted of poorly liberated particles of galena, chalcopyrite, and sphalerite – most likely because they were locked in pyrite particles, which themselves were well liberated (Fig. 6) – while in the final 5 min of flotation, more liberated particles are recovered.

This is especially relevant for the galena-bearing particles which showed the lowest recoveries. It corroborates the results presented in Fig. 12 where it is observed that the Pb grade increases toward the end of the flotation time. Furthermore, changes in the froth structure after the removal of large amounts of material might also affect the recovery of fine particles through entrainment (Hoang et al., 2018).

It is also noted that Tail 4 contains a high percentage of liberated galena particles that were not recovered. Therefore, further investigation on the grain size distribution of the liberated galena in Tail 4 was performed via MLA and the results are presented in Fig. 22. Note that 100% of the grains are below 4.8 μm. The smallest grains identified are below 2 μm and represent about 10% of the mass. However, there are probably also finer-grained galena particles that could not be identified with MLA, which could imply a higher percentage of particles smaller than 2 μm in reality, making the galena even more difficult to float.

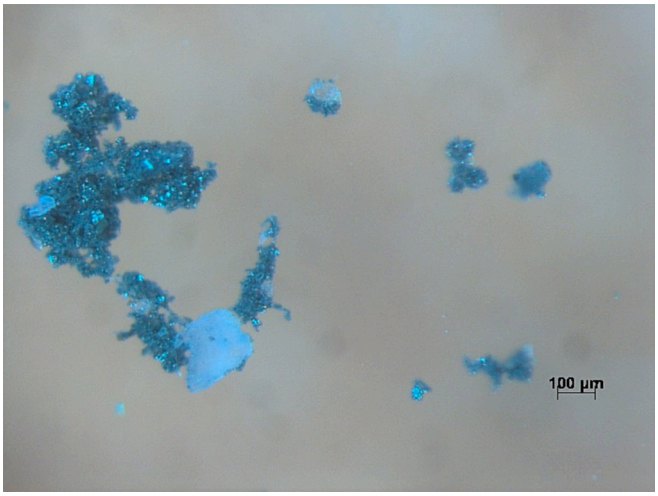

Fig. 15. Microscope image of flocs formed after the addition of SFN100 (50 g/t) to a suspension of Neves Corvo tailings (sample A) in pH 8.

4. Discussion

4.1. Data quality

Cu, S, and Zn MLA back-calculated assays were in good agreement with the chemical assay for the samples, while MLA underestimated the Pb content in all studied process samples (Fig. 5). This could potentially be due to (1) an insufficient number of particles measured during the MLA measurements and/or (2) the complex ore textures at Neves-Corvo (Gaspar and Pinto, 1991) having ultrafine galena grains locked in sulfides or gangue minerals that the microscopic observations could not capture. For these reasons, in this study, we considered the MLA data for sphalerite, pyrite, and chalcopyrite as sufficient quality. For Pb/galena, MLA results may be indicative of truth, but cannot be taken to derive

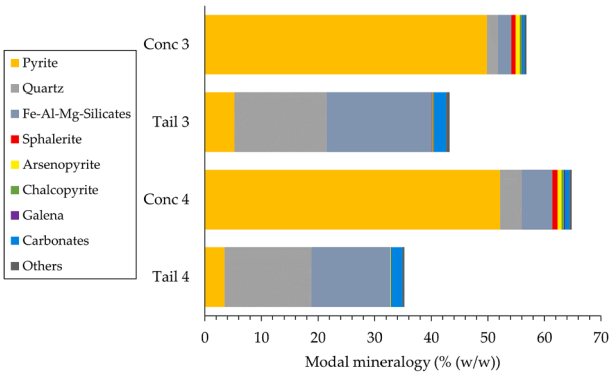

Fig. 18. Modal mineralogy (% (w/w)) of concentrate (Conc 3–4), and tailings (Tail 3–4) samples, obtained with MLA. The modal mineralogy of each product does not sum to 100%, since it illustrates the relative mass flow of the different minerals.

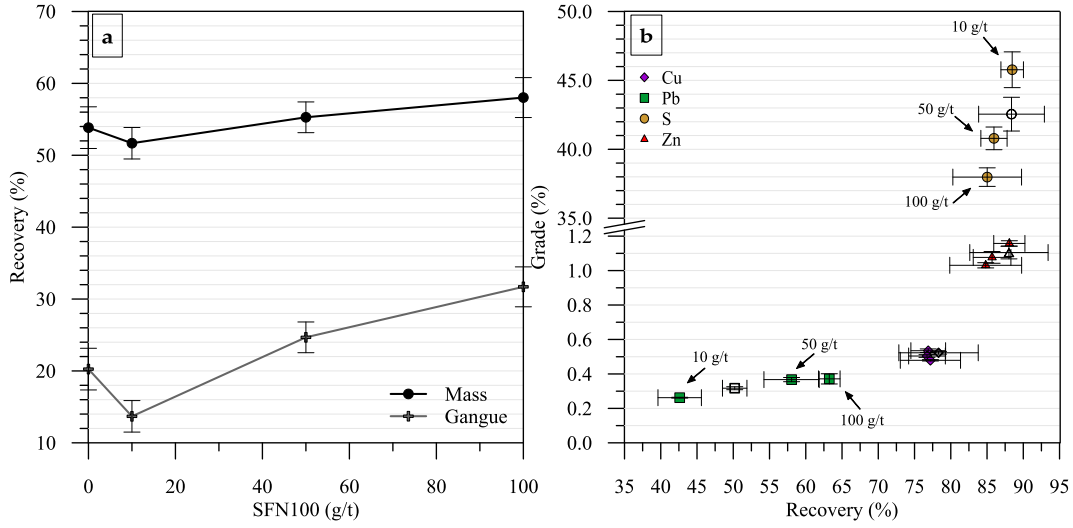

Fig. 16. Flotation of the undersize fraction (sample C). (a) Mass and gangue recovery versus SFN100 dosage and b) recovery versus grade of Cu, Pb, Zn, and S without flocculant (unfilled symbols) and with 10 g/t, 50 g/t, and 100 g/t SFN100. The experiments were performed using 300 g/t CuSO4, 100 g/t SIBX, 100 g/t MIBC, pH 6, 25% solids, and 5 min flotation.

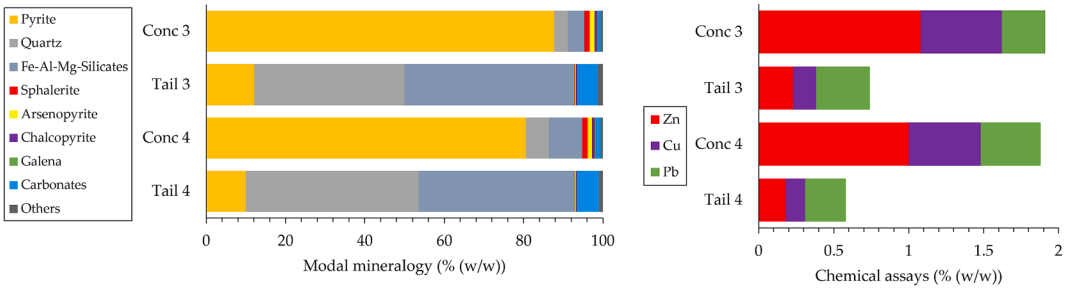

Fig. 17. Modal mineralogy (% (w/w)) and Zn, Cu, and Pb assays of feed (B and C), concentrate (Conc 3–4), and tailings (Tail 3–4) samples after 10 min of flotation, obtained, respectively, with MLA and ICP-OES.

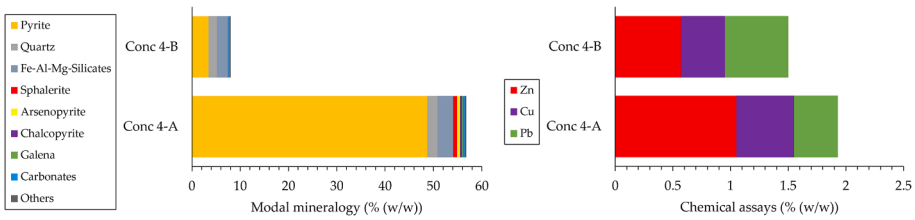

Fig. 19. Modal mineralogy (% (w/w)) and chemical assays (% (w/w)) of Conc 4-A (0–5 min flotation) and Conc 4-B (5–10 min flotation) adding 50 g/t SFN100, obtained, respectively, via MLA and ICP-OES. The modal mineralogy of each product does not sum to 100%, since it illustrates the relative mass flow of the different minerals.

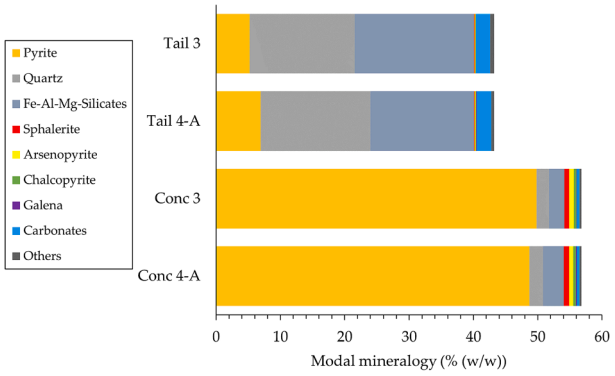

Fig. 20. Modal mineralogy (% (w/w)) of concentrate and tailings samples from conventional (Conc 3 and Tail 3) and floc flotation (Conc 4-A and Tail 4-A) tests, obtained with MLA. The modal mineralogy of each product does not sum to 100%, since it illustrates the relative mass flow of the different minerals.

exact quantitative conclusions, and must be considered semi-quantitative. Previous research observed that mineral abundances and ore textures play an important role in accurate characterization via MLA, with samples with low-grade and finely inter-grown minerals contributing to higher uncertainties and being much more challenging to characterize than coarse mineral grains and abundant minerals (Blannin et al., 2021; Bevandić et al., 2022).

4.2. Characterization

A detailed characterization of the tailings sample was undertaken through chemical, mineralogical, and physical methods to assess the relations between mineralogy, grade, and textures. The investigations show that the Neves Corvo sample (A) is a high-pyrite tailings material, with valuable Cu-, Zn-, and Pb-sulfide minerals present at low concentrations. The sample has a broad particle size distribution (D80 = 66 μm), with abundant fine and ultra-fine (<10 μm) particles.

Whereas pyrite was rejected and hence reported to the tailings, fine particles of Cu-, Zn-, and Pb-sulfide minerals likely entered the tailings due to the poor floatability of fine and ultrafine particles; flotation efficiency and kinetics of particles below 10 μm suffer severely from low particle bubble collision during flotation (Wills and Finch, 2016). Additionally, the Cu-, Zn-, and Pb-sulfides may be interlocked with pyrite particles and therefore report to the tailings. Notably, the MLA analysis of the Neves Corvo tailings revealed the valuable minerals (chalcopyrite, galena, and sphalerite) are not fully liberated (Fig. 7), despite the fine particle size of the samples. Previous research has shown that the Neves Corvo ore textures impose a practical problem in the recovery of the metals since the ore requires very fine grinding to achieve liberation, which adversely affects the froth flotation processing of the ore (Gaspar and Pinto, 1991).

The sample characterization suggests that selective flotation for the valuable minerals (chalcopyrite, galena, and sphalerite) would likely not be practical as only a small percentage of these minerals are liberated (Fig. 8) or intergrown with pyrite. Re-milling the tailings to liberate the non-iron sulfides would not be effective because of the resulting problems in flotation due to further grain size reduction and extremely high energy consumption. Furthermore, considering the high floatability of pyrite, its more favorable size distribution, and that it represents 40–60 wt% of the samples (Fig. 4) the selective flotation of the Cu-, Zn-, and Pb-sulfide minerals is likely to be difficult.

4.3. Classic flotation

The results of preliminary flotation tests (300 g/t copper sulfate, 100 g/t SIBX, 100 g/t MIBC, pH 6, and 25 % solids) showed promising potential for the bulk recovery of sulfide minerals from the Neves-Corvo material, with S recoveries reaching 93.6 % (Fig. 9) and circa 2.46 % combined Cu-Pb-Zn grade within 16 min flotation. The resulting new tailings represent 40 % of the original mass but contain only 6.0 % - 7.0 % of the original sulfur. Toxic element concentrations and AMD potential have hence been drastically reduced.

Thereafter, the same conditions were used in the flotation of samples B (coarse fraction) and C (fine fraction). In terms of recovery, the results obtained from the flotation of C were very similar to those of sample A. Recoveries of S reached 95.3 % with a lower combined Cu-Pb-Zn grade of 1.85 %. The resulting new tailings represent 37 % of the mass of sample C but contain only 4.0 % - 5.4 % of the initial sulfur in sample C.

On the other hand, the coarser sample B always yielded faster flotation rates and enabled a more selective flotation of the S-bearing minerals, with S recoveries reaching 96.6 % and combined Cu-Pb-Zn grades of around 3.66 % within 10 min. The resulting new tailings represent 49 % of sample B's mass but contain only 2.9 % - 4.1 % of the initial sulfur in sample B. Further tests using half of the collector dosage (50 g/t) and a shorter time (5 min) demonstrated that the flotation of the oversize particles under these conditions still produces cleaner tailings than the flotation of the finer particles. It corroborates the fact that smaller particles consume higher collector dosages due to their higher specific surface area (Demers, 2005) but also that coarser particles float faster, demonstrating that slow rates are the main problem with fine particles.

Most likely, the worse flotation performance obtained for samples A and C can be attributed to the ultrafine hydrophobic mineral particles not being efficiently collected by air bubbles (Wills and Finch, 2016). The low flotation rate of fine particles is a well-known phenomenon and one of the major causes of the losses of sulfides to the tailings. Surface chemistry studies also indicated that fine particles are more heavily oxidized and, consequently, in the case of strong oxidation, flotation efficiency is lower (Demers, 2005).

Especially for Zn, the flotation of sample A shows considerably higher recoveries than that of sample C for most of the flotation time (Fig. 11a). The differences between the concentrate of samples A and C can be attributed to the faster flotation kinetics and higher sphalerite content of the coarse material fraction.

Among the target elements, Pb presented the lowest recovery and grade enhancement in all the flotation approaches applied in this research, which is likely due to the poorer flotation efficiency of the

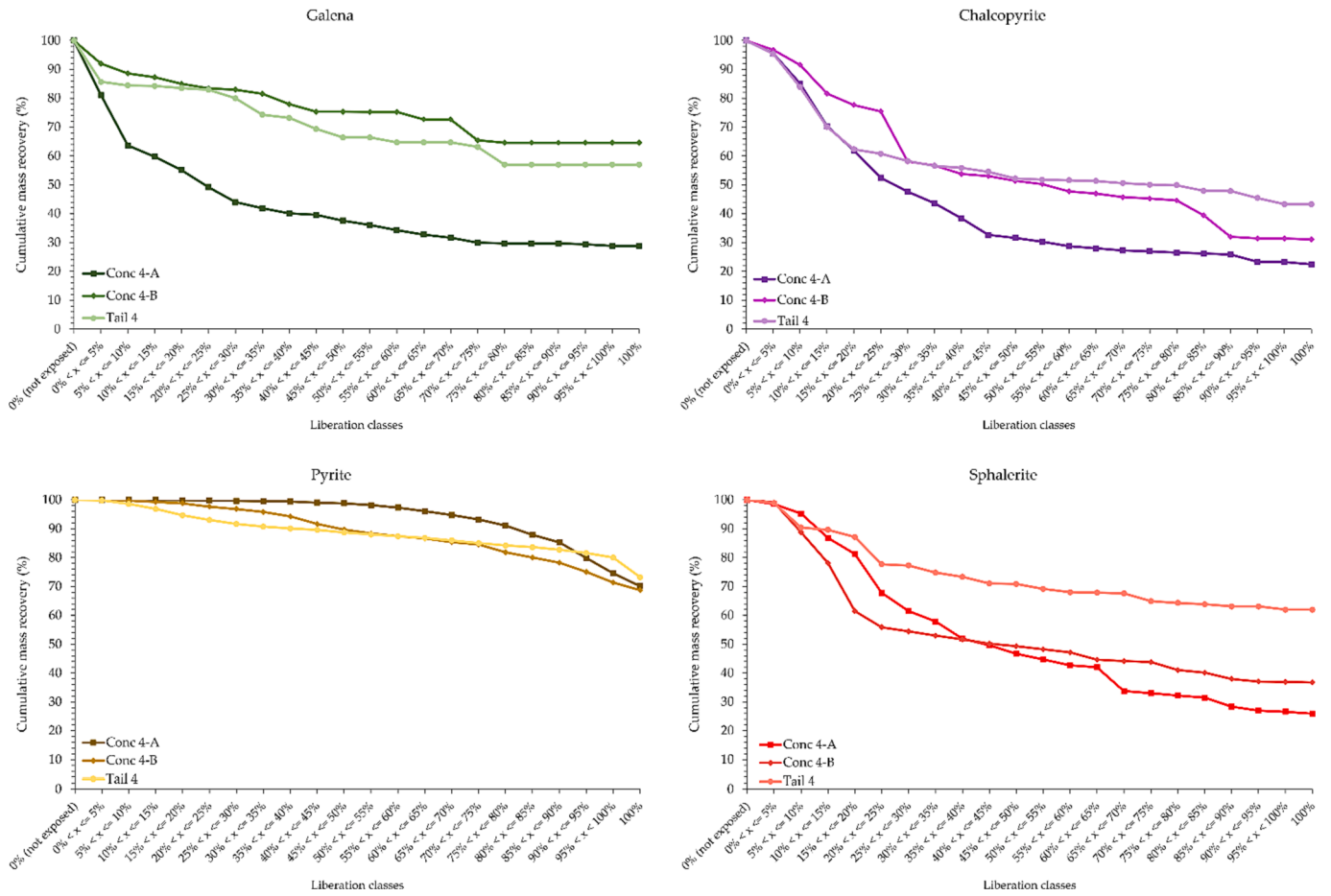

Fig. 21. Liberation by free surface of galena, chalcopyrite, pyrite, and sphalerite on the Conc 4-A (0–5 min), Conc 4-B (5–10 min), and Tail 4 (10 min). The flotation was performed using 300 g/t CuSO4, 50 g/t N100, 100 g/t SIBX, 100 g/t MIBC, pH 6, and 25% solids.

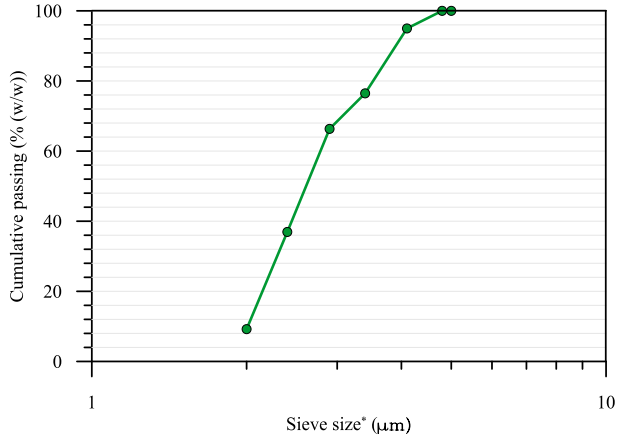

Fig. 22. Liberated galena grain size distribution in Tail 4, obtained with MLA. *ECD (equivalent circle diameter).

ultrafine galena particles and the reduced entrainment recovery due to its high specific gravity. As our data shows, over 52.5 % of the Pb is found in particles smaller than 5 μm (Table 3), and the investigation of the galena liberation revealed that 100 % of the liberated grains in the tailings are below 4.8 μm.

It is noteworthy that the grades of Cu, Pb, and (sometimes) Zn in the concentrate did not follow the typical trend in flotation where they decrease as recovery increases. As seen in this study, the grade/recovery trends observed showed consistent values of grade, even increasing trends, especially for Pb, suggesting that the same ratio of those elements report to the overflow throughout the experiment. This phenomenon could be explained by the faster flotation of locked chalcopyrite, sphalerite, and galena in pyrite particles, followed by the flotation of liberated particles of those minerals, which are smaller and hence float later.

The presented flotation route for the reprocessing of the Neves Corvo tailings focuses on mass reduction, separation of hazardous elements, and generation of sulfide-rich concentrates. The study showed that the split of the material into two-size fractions through wet sieving is possible due to the relatively broad particle size distribution of the tailings. Classic flotation tests proved that sulfide concentrates can be produced either using a single route or a two-route process, nevertheless, with higher selectivity and recovery for the coarse particle route, due to their physical properties.

4.4. *Floc flotation*

It is known that increasing particle sizes can allow for faster flotation rates and improve selectivity. Therefore, selective flocculation using a neutral polyacrylamide, SN100, was attempted, aiming to increase the size of sulfide mineral particles before flotation. Polyacrylamides are widely used polymers in many industries and are effective as flocculants in the mineral processing industry (Boulton et al., 2001; Sresty and Somasundaran, 1980; Oliveira, 2016).

The addition of 50 g/t SFN100 in the flotation of sample C obtained a higher mass pull and an increase in the pyrite recovery from 56.8 % to 64.8 %, however, it also produced a dilution of the concentrate (Fig. 17). These observations suggest that the flocculant might have a depressant

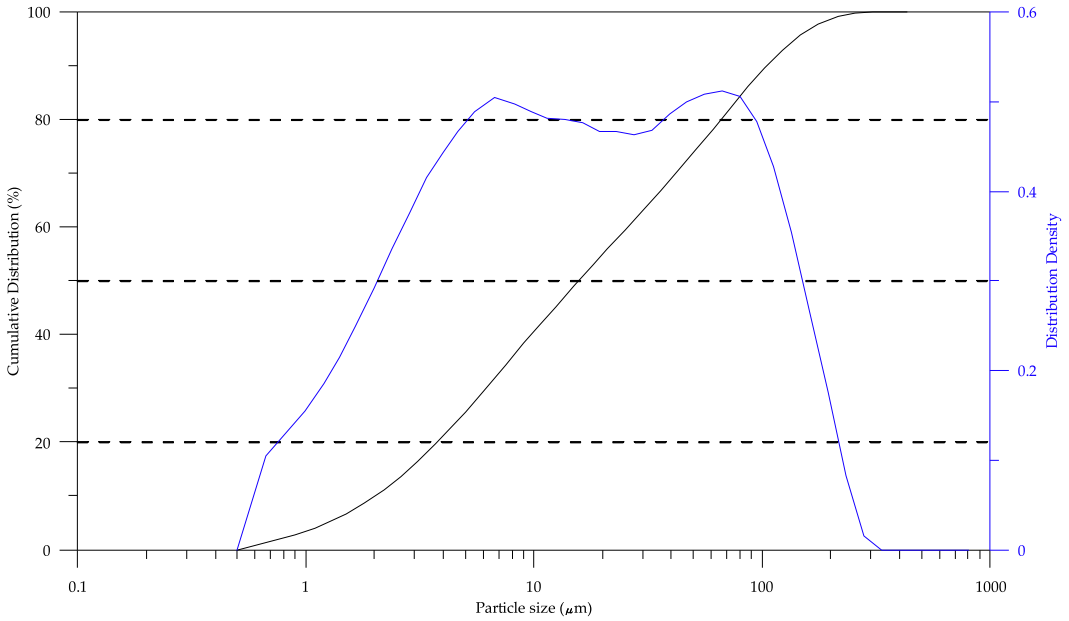

Fig. A1. Particle size distribution of Neves Corvo tailings (sample A), as measured by laser diffraction analysis.

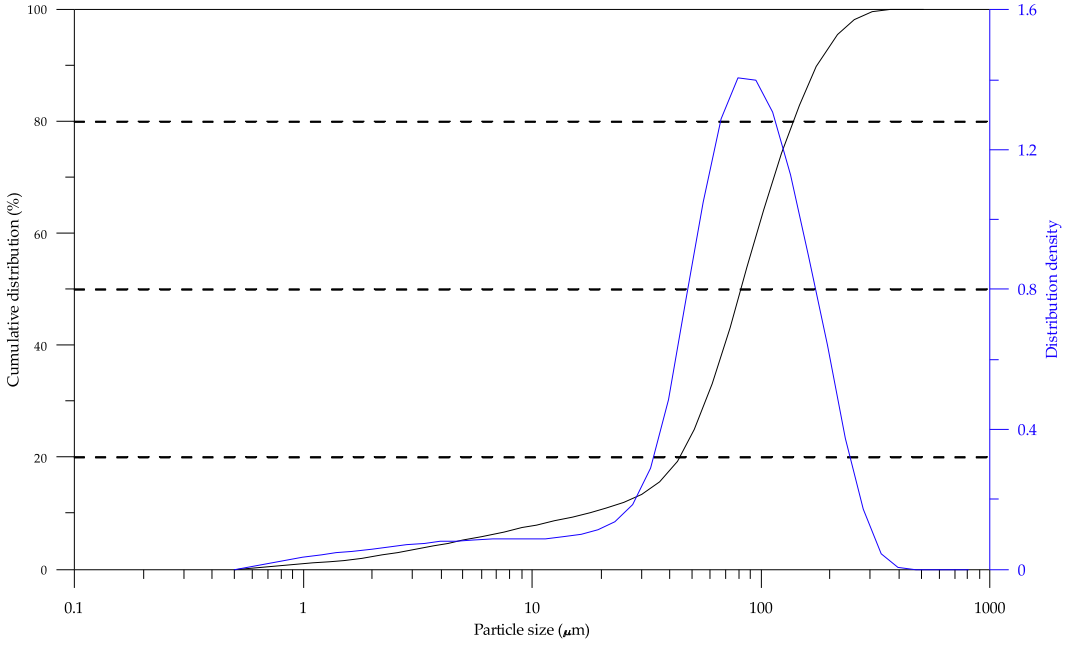

Fig. A2. Particle size distribution of the oversize from Neves Corvo tailings (sample B), as measured by laser diffraction analysis.

effect on the pyrite surface and/or indicate that the flocculant's effect on the froth, and thus entrainment, is much more dominant than any collection efficiency improvements. Many factors can lead to these results, such as 1) the coverage of the adsorption sites of the collector by the flocculant (Somasundaran, 1978; Wightman et al., 2000; Boulton et al., 2001), 2) the entrapment of gangue particles in the flocs (Lu et al., 2005), and 3) the non-selective adsorption-flocculation of the minerals caused, for instance, by surface contamination (e.g. during grinding) (Rubio and Marabini, 1987).

Previous studies on the flocculation of pyrite, chalcopyrite, and quartz in pH 8–10, using an anionic polyacrylamide (Superfloc A130) (Coelho Braga de Carvalho et al., 2021) and the neutral polyacrylamide SFN100 (unpublished results) found that both flocculants had a low effect on quartz suspensions and a high effect on sulfide mineral suspensions. However, the lower the pH, the better the quartz flocculation. Therefore, it is likely that pH 6 (which was the best for the sulfide flotation) did not provide a sufficiently high pH to enable flocculation to act selectively on the sulfide minerals. More test work is required to investigate this hypothesis.

It is known from previous studies that polyacrylamide polymers can depress sulfide minerals (Somasundaran, 1978; Boulton et al., 2001). Wightman and coworkers also found that the addition of a high molecular weight polymer before the collector reduced the recovery of galena which they attributed to several reasons, for example, the presence of polymer on the mineral surface inhibiting collector adsorption (Wightman et al., 2000). Somasundaran reports the flotation of sphalerite to be enhanced by polyacrylamide polymers up to certain concentrations, and to be depressed above these levels (Somasundaran,

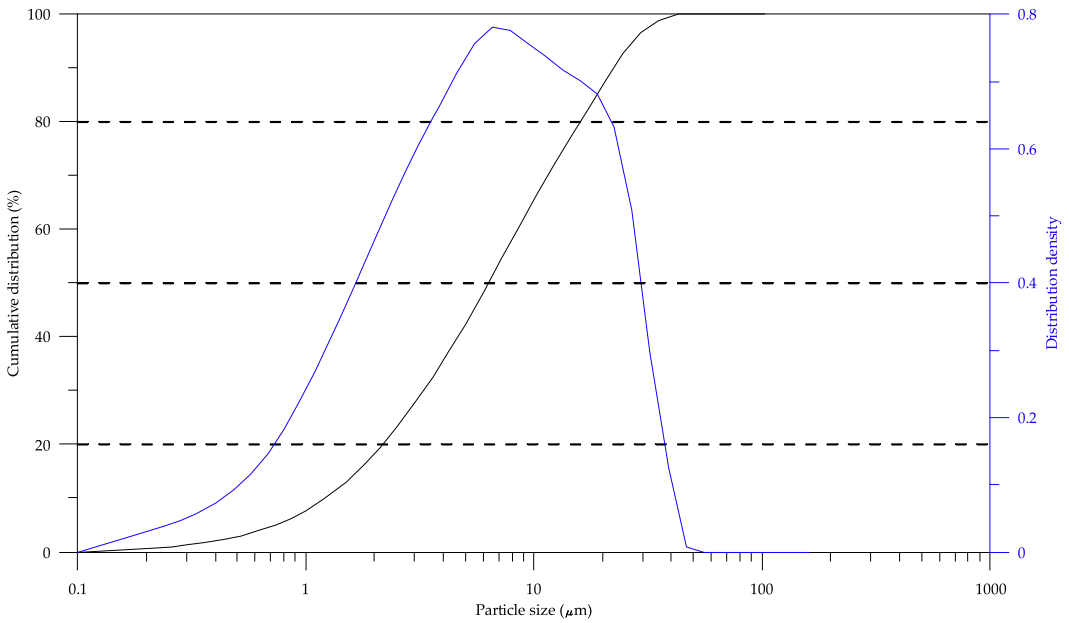

Fig. A3. Particle size distribution of the undersize of Neves Corvo tailings (sample C), as measured by laser diffraction analysis.

Table B1
Chemical assays of the granulochemical analysis of Neves Corvo tailings (sample A), as measured by ICP-OES.

Size range	Retained	Ag	Al	As	Ba	Ca	Cd	Co	Cr	Cu	Fe	K	Mg
μm	(%)	ppm	ppm	ppm	ppm	ppm	ppm	ppm	ppm	ppm	ppm	ppm	ppm
150–200	5.33	18	31,643	1537	109	3184	56	68	70	2637	166,972	3181	9690
100–150	8.71	20	31,434	1975	89	3861	52	89	48	3149	203,797	2687	11,067
90–100	1.87	24	26,170	2869	75	3179	53	122	58	3861	247,994	2281	9413
80–90	3.83	23	24,983	3146	84	3692	48	136	48	4420	261,843	2158	9346
63–80	5.60	21	25,074	3585	87	3714	40	156	36	4556	275,341	2134	8886
40–63	14.52	18	22,293	4359	89	3053	25	185	55	3831	293,445	1982	8194
32–40	2.23	19	13,942	6264	80	2691	20	243	60	3378	350,803	1265	5596
25–32	3.74	16	20,789	5476	99	3018	16	212	71	2877	315,802	1830	7505
20–25	5.98	17	20,227	5589	99	2909	13	223	79	2675	325,350	1797	7261
15–20	3.38	14	25,394	5446	96	1830	13	203	29	2845	302,968	3154	9822
10–15	9.35	14	20,538	5363	95	1533	12	222	26	2505	329,254	2519	7020
5–10	2.64	17	26,236	5298	116	898	13	208	40	3002	304,877	3694	7464
<5	32.83	31	41,195	6062	157	905	13	190	99	4521	283,348	6477	10,203

Size range	Retained	Mn	Na	Ni	P	Pb	S	Sb	Si	Sr	Ti	Zn
μm	(%)	ppm	ppm	ppm	ppm	ppm	ppm	ppm	ppm	ppm	ppm	ppm
150–200	5.33	609	546	219	159	3568	160,518	99	239,444	17	1256	22,362
100–150	8.71	677	576	123	193	3448	198,817	117	192,268	16	1206	20,682
90–100	1.87	636	502	180	175	3871	260,137	155	155,401	16	1060	21,106
80–90	3.83	646	471	160	161	3342	269,807	155	146,706	15	1065	19,834
63–80	5.60	635	487	80	181	2923	278,735	157	146,320	15	1295	15,702
40–63	14.52	629	484	163	184	2147	303,650	154	123,001	20	1033	9874
32–40	2.23	510	372	240	165	1894	381,199	174	81,603	14	807	7228
25–32	3.74	606	541	244	228	1689	342,130	154	111,018	16	1086	5731
20–25	5.98	609	436	266	220	1553	356,776	159	103,975	16	1100	4925
15–20	3.38	624	793	23	172	1422	318,780	151	115,531	17	1135	5096
10–15	9.35	548	852	34	183	1276	310,493	177	94,699	14	978	4546
5–10	2.64	506	1229	61	170	1448	296,627	261	107,428	15	843	5200
<5	32.83	574	2083	46	251	5276	235,001	379	104,731	25	1119	6354

1978). The better results at low concentrations were credited to a potential fractional surface coverage and consequent flocculation. Conversely, the worst results under higher dosages were attributed to a more complete coverage that retarded flocculation and possibly collector adsorption on the particles and thus flotation. However, the exact reasons for the activating effect at low concentrations and the depressing effect at higher concentrations were not clear.

Increasing the particle size through polymeric agglomeration proved to be challenging for the Neves Corvo tailings, especially due to the high grade of pyrite in the samples, which inevitably causes entrapment of the gangue particles during floc formation. Lu and co-workers postulated that a major problem hindering selective flocculation with high-solid-content slurries (>20%) results from particle entrapment. This happens when the formation rate, size, and settling rate of flocs are comparatively high, which inevitably produces a certain degree of entrapment or entrainment of the undesired material (Lu et al., 2005). The phenomenon is aggravated when the flocculated component is present at a higher concentration (high grade) compared to the non-flocculated material (Rubio and Marabini, 1987).

A possible remedy to these effects is the addition of washing steps to

Table C1
The list of minerals identified by MLA with mineral groupings.

Group	Minerals
Carbonates	Ankerite, Calcite, Dolomite, Magnesite-Fe, Magnesite-Siderite[1], Siderite-Magnesite[2], Siderite-Mn, Siderite-Mn-Mg
Oxides	Cassiterite, Rutile
Phosphates	Apatite
Silicates	Quartz, Fe-Al-Mg-Silicate, Al-Silicate 1[3], Al-Silicate 2[4], Al-Silicate 3[5], Fe-Al-Silicate, Fe-Al-Silicate 2, Muscovite, Orthoclase, Plagioclase, Zircon
Sulfates	Barytes, Gypsum, Jarosite
Sulfides	Pyrite, Sphalerite, Sphalerite with loFe, Chalcopyite, Galena, Galena-Se, Arsenopyrite, Bornite, Covellite, Danielsite/Balkanite, Roquesite, Sakuraiite, Stannite, Stannite, Stannite-Ag, Stannoidite
Sulfosalts	Bournonite, Enargite, Tennantite, Tetrahedrite

[1] Mixed-spectra between Magnesite and Siderite (2:1).
[2] Mixed-spectra between Siderite and Magnesite (1.5:1).
[3] Al-Silicate (Al:Si 1:2).
[4] Al-Silicate (Al:Si 2:1).
[5] Al-Silicate (Al:Si 1:1).

remove the entrained particles. In the work of Attia on the development of a treatment for complex copper ore, multiple stages of flocculation and redispersion were necessary to release trapped particles and obtain satisfactory enrichment of the ore (Attia, 1977). In the work of Sresty and Somasundaran, who used modified polymers, cleaning the selectively flocculated product by simple redispersion in water improved the separation efficiency (Sresty and Somasundaran, 1980). In the current research, the use of washing steps was not tested but could have the potential to improve the results.

4.5. General implications

A rough concept for the (re-)processing of Neves Corvo tailings was deduced based on the characterization of the material, as well as the objectives to reduce AMD potential and toxic element content, and potentially enable the recovery of valuable Cu-, Zn-, and Pb-sulfide minerals. We demonstrated that by using classic flotation, the potentially valuable minerals can be concentrated, and the harmful elements can be strongly depleted in the generated residues. We recovered 93.6%

Table D1
First order rate constant (k) and recovery after infinite flotation time (R_∞) (Wills and Finch, 2016), for Cu, Pb, S, and Zn. The experiments were performed using 300 g/t CuSO4, 100 g/t SIBX, 100 g/t MIBC, 25% solids, and pH 6.

Sample	Cu k (min^{-1})	Cu R_∞	Pb k (min^{-1})	Pb R_∞	S k (min^{-1})	S R_∞	Zn k (min^{-1})	Zn R_∞
A	0.59	0.81	0.48	0.67	0.76	0.86	0.98	0.86
B	2.46	0.87	2.04	0.72	3.01	0.95	2.61	0.94
C	0.43	0.85	0.25	0.61	0.57	0.91	0.43	0.89

Table E1
Raw data from the experiment using sample A, 300 g/t CuSO4, 100 g/t SIBX, 100 g/t MIBC, 25% solids, and pH 6. Chemical assays were obtained via ICP-OES.

Time (min)	Product	Mass recovery (%)	Mass recovery (SD)	Cu (%)	Cu (SD)	Fe (%)	Fe (SD)	Pb (%)	Pb (SD)	S (%)	S (SD)	Zn (%)	Zn (SD)
0.5	Concentrate	19.1	0.15	0.55	0.007	39.9	0.179	0.42	0.005	46.3	0.338	2.00	0.070
0.5	Tailing	80.9	0.15	0.32	0.004	23.8	0.123	0.34	0.014	21.0	0.199	0.73	0.029
1	Concentrate	26.2	0.03	0.55	0.011	39.9	0.191	0.41	0.010	45.9	0.167	1.93	0.093
1	Tailing	73.8	0.03	0.30	0.001	22.3	0.131	0.34	0.013	18.7	0.230	0.64	0.014
2	Concentrate	34.1	0.89	0.55	0.012	39.7	0.191	0.41	0.008	45.6	0.065	1.86	0.091
2	Tailing	65.9	0.89	0.27	0.003	20.3	0.421	0.33	0.015	15.7	0.164	0.52	0.023
4	Concentrate	43.2	0.61	0.55	0.009	39.1	0.105	0.41	0.007	44.6	0.310	1.77	0.073
4	Tailing	56.8	0.61	0.23	0.003	17.6	0.223	0.31	0.017	11.6	0.120	0.38	0.020
6	Concentrate	48.5	0.28	0.55	0.008	38.5	0.062	0.42	0.008	43.6	0.206	1.70	0.064
6	Tailing	51.5	0.28	0.20	0.002	16.0	0.143	0.30	0.017	9.1	0.268	0.30	0.015
8	Concentrate	52.2	0.63	0.55	0.008	38.0	0.111	0.43	0.007	42.7	0.266	1.64	0.066
8	Tailing	47.8	0.63	0.17	0.004	14.8	0.267	0.28	0.019	7.5	0.110	0.25	0.019
13	Concentrate	58.2	0.03	0.54	0.011	36.8	0.191	0.43	0.010	40.8	0.167	1.50	0.070
13	Tailing	41.8	0.03	0.13	0.001	13.1	0.131	0.24	0.013	5.3	0.230	0.19	0.014
16	Concentrate	60.9	0.05	0.54	0.006	36.1	0.061	0.43	0.008	39.7	0.039	1.49	0.048
16	Tailing	39.1	0.05	0.11	0.000	12.6	0.169	0.24	0.018	4.2	0.330	0.17	0.012

Time (min)	Product	Cu recovery (%)	Cu recovery (SD)	Fe recovery (%)	Fe recovery (SD)	Pb recovery (%)	Pb recovery (SD)	S recovery (%)	S recovery (SD)	Zn recovery (%)	Zn recovery (SD)
0.5	Concentrate	28.6	0.2	28.3	0.4	22.5	0.7	34.2	0.2	39.2	0.3
0.5	Tailing	71.4	0.2	71.7	0.4	77.5	0.7	65.8	0.2	60.8	0.3
1	Concentrate	39.2	0.3	38.9	0.3	30.2	0.3	46.6	0.4	51.8	0.6
1	Tailing	60.8	0.3	61.1	0.3	69.8	0.3	53.4	0.4	48.2	0.6
2	Concentrate	50.9	0.8	50.2	1.6	39.2	1.6	60.1	1.2	64.9	0.8
2	Tailing	49.1	0.8	49.8	1.6	60.8	1.6	39.9	1.2	35.1	0.8
4	Concentrate	64.7	0.5	62.9	0.8	50.3	1.6	74.6	0.1	78.2	0.6
4	Tailing	35.3	0.5	37.1	0.8	49.7	1.6	25.4	0.1	21.8	0.6
6	Concentrate	72.6	0.1	69.4	0.4	57.2	1.3	81.8	0.3	84.2	0.3
6	Tailing	27.4	0.1	30.6	0.4	42.8	1.3	18.2	0.3	15.8	0.3
8	Concentrate	77.9	0.6	73.6	0.8	62.3	1.8	86.2	0.0	87.7	0.6
8	Tailing	22.1	0.6	26.4	0.8	37.7	1.8	13.8	0.0	12.3	0.6
13	Concentrate	85.7	0.2	79.6	0.4	71.4	0.6	91.4	0.1	91.8	0.3
13	Tailing	14.3	0.2	20.4	0.4	28.6	0.6	8.6	0.1	8.2	0.3
16	Concentrate	88.6	0.1	81.8	0.2	74.1	1.0	93.6	0.5	93.1	0.2
16	Tailing	11.4	0.1	18.2	0.2	25.9	1.0	6.4	0.5	6.9	0.2

Table E2
Raw data from the experiment using sample B, 300 g/t CuSO4, 100 g/t SIBX, 100 g/t MIBC, 25% solids, and pH 6. Chemical assays were obtained via ICP-OES.

Time (min)	Product	Mass recovery (%)	Mass recovery (SD)	Cu (%)	Cu (SD)	Fe (%)	Fe (SD)	Pb (%)	Pb (SD)	S (%)	S (SD)	Zn (%)	Zn (SD)
0.5	Concentrate	37.3	0.44	0.61	0.020	39.5	1.371	0.40	0.040	46.0	1.260	2.67	0.355
0.5	Tailing	62.7	0.44	0.20	0.006	14.9	0.202	0.23	0.006	8.7	0.363	0.63	0.044
1	Concentrate	42.4	0.73	0.62	0.017	39.3	1.308	0.41	0.038	45.7	1.210	2.72	0.315
1	Tailing	57.6	0.73	0.16	0.004	12.9	0.147	0.21	0.004	5.6	0.246	0.41	0.032
2	Concentrate	46.1	0.96	0.62	0.016	38.9	1.344	0.42	0.036	45.1	1.262	2.73	0.301
2	Tailing	53.9	0.96	0.12	0.002	11.5	0.150	0.19	0.001	3.4	0.194	0.24	0.011
4	Concentrate	48.9	0.59	0.62	0.015	38.2	1.139	0.43	0.032	44.1	0.965	2.69	0.302
4	Tailing	51.1	0.59	0.09	0.005	10.6	0.228	0.17	0.005	2.1	0.284	0.14	0.011
6	Concentrate	49.9	0.48	0.62	0.016	37.8	1.062	0.44	0.030	43.5	0.852	2.66	0.302
6	Tailing	50.1	0.48	0.08	0.006	10.4	0.247	0.16	0.006	1.8	0.299	0.12	0.011
8	Concentrate	50.6	0.59	0.62	0.015	37.6	1.089	0.44	0.030	43.1	0.898	2.63	0.296
8	Tailing	49.4	0.59	0.08	0.005	10.3	0.229	0.15	0.005	1.7	0.266	0.11	0.007
10	Concentrate	51.2	0.53	0.62	0.016	37.3	1.049	0.44	0.029	42.7	0.836	2.61	0.297
10	Tailing	48.8	0.53	0.08	0.005	10.2	0.238	0.14	0.006	1.6	0.269	0.11	0.006

Time (min)	Product	Cu recovery (%)	Cu recovery (SD)	Fe recovery (%)	Fe recovery (SD)	Pb recovery (%)	Pb recovery (SD)	S recovery (%)	S recovery (SD)	Zn recovery (%)	Zn recovery (SD)
0.5	Concentrate	64.5	0.5	61.1	0.7	50.5	2.3	75.8	0.9	71.4	1.7
0.5	Tailing	35.5	0.5	38.9	0.7	49.5	2.3	24.2	0.9	28.6	1.7
1	Concentrate	74.1	0.6	69.1	0.3	58.8	2.5	85.6	0.5	82.9	1.0
1	Tailing	25.9	0.6	30.9	0.3	41.2	2.5	14.4	0.5	17.1	1.0
2	Concentrate	81.3	0.8	74.3	0.2	65.4	2.7	91.9	0.3	90.7	0.9
2	Tailing	18.7	0.8	25.7	0.2	34.6	2.7	8.1	0.3	9.3	0.9
4	Concentrate	86.4	0.0	77.4	0.5	71.3	1.4	95.2	0.6	94.7	0.3
4	Tailing	13.6	0.0	22.6	0.5	28.7	1.4	4.8	0.6	5.3	0.3
6	Concentrate	88.0	0.2	78.4	0.6	73.7	1.0	95.9	0.6	95.5	0.2
6	Tailing	12.0	0.2	21.6	0.6	26.3	1.0	4.1	0.6	4.5	0.2
8	Concentrate	88.8	0.1	78.9	0.5	75.2	1.0	96.3	0.5	95.9	0.3
8	Tailing	11.2	0.1	21.1	0.5	24.8	1.0	3.7	0.5	4.1	0.3
10	Concentrate	89.5	0.1	79.3	0.5	76.5	0.8	96.6	0.6	96.2	0.3
10	Tailing	10.5	0.1	20.7	0.5	23.5	0.8	3.4	0.6	3.8	0.3

of the sulfur contained in the original tailings and decreased the S grade from 25.9% to 4.2%. In addition, we obtained recoveries of 88.6% Cu, 74.1% Pb, and 93.1% Zn, with grades of 0.54% Cu, 0.43% Pb, and 1.49% Zn in the concentrate. Separating non-ferrous sulfide concentrates was not tested due to the similarity of the sulfide surfaces, the dominance of intergrowths, and low concentrations in the feed. Overall, the large proportion of fine and ultrafine particles in the tailings caused a low flotation rate. It also strongly influenced the recovery of gangue minerals through entrainment and entrapment, lowering selectivity.

A further attempt towards a more selective flotation and the generation of residues with lower S content was made through the division of Neves Corvo tailings by particle size, and use of two different flotation routes. The flotation of the fraction with a more suitable size for flotation provided: a) higher sulfide recoveries, b) higher combined Cu-Pb-Zn grades in the concentrate (3.66%), c) cleaner residues (1.6% S), d) faster flotation rate, and e) lower reagent consumption. Likewise, the results from the fine particle flotation allowed lower S content in the residues (3.4% S) compared to the flotation of the original material. Therefore, the use of a conventional two-route approach indicates significant advantages compared to a single route.

The resulting flotation products may have to undergo further treatment to conform to marketing and/or disposal specifications. The sulfide concentrates produced, particularly from the coarser fraction of the material, contain valuable elements such as Cu, Pb, and Zn at levels similar to commercial ores (this is particularly true for copper since porphyry ores have Cu contents of approximately 0.5 %), which could be separated in subsequent (bio)hydrometallurgical steps. Schueler and coworkers, for instance, obtained recoveries of 66.8% copper, 84.1% zinc, and 93.9% lead in leaching tests conducted with Neves Corvo tailings samples (Schueler et al., 2021). In their research, about 20% and 50% of the iron and arsenic content, respectively, was also leached. During hydrometallurgy, the high iron content could lead to increased acid consumption (Römer et al., 2018).

The generated tailings consist mostly of silicate and carbonate minerals (86–96%), and the remaining sulfides, resulting in a significantly lower potential for acid rock drainage (Parbhakar-Fox et al., 2017). Therefore, less neutralizing agent would be required to eliminate the remaining hazards if these tailings were to be deposited in a tailings storage facility. The use of the tailings as a construction raw material could be facilitated by the further removal of the sulfides, in a second flotation step, or a (bio)hydrometallurgical step. However, investigations on the use of uncleaned Neves Corvo waste rock – with similar levels of sulfide minerals – suggest that the generated tailings present potential for use as non-shaped building products as a substitute for primary resources (Veiga Simão et al., 2021).

The investigations on the use of floc flotation for the finer particles increased the mass pull in the concentrate from 56.8% to 64.8% leading to slightly higher recoveries of sulfides and a noticeable increase in the recovery of quartz and Fe-Al-Mg-Silicates. It indicates that at the dosage used, the flocculant might have a depressing effect on the pyrite surface, such that flotation becomes less selective as flocculant is added.

For the further investigations, we recommend experiments using: a) lower solid percentages and/or a higher pH in a flocculation step before flotation, b) the investigation of selective flocculants with functional groups with a greater affinity towards the sulfide minerals, as well as c) the application of other methods for particle agglomeration and fine flotation (e.g. column flotation) to improve the performance, particularly in terms of selectivity, of the floc-flotation.

5. Summary and conclusions

This research showed a case study on the (re-)processing of the Neves Corvo mine tailings. The major results can be summarized as follows:

Pyrite constitutes the main mineral present in the tailings. Most of the valuable ore minerals are finely intergrown with pyrite and are recoverable by bulk sulfide flotation.

Table E3
Raw data from the experiment using sample C, 300 g/t CuSO4, 100 g/t SIBX, 100 g/t MIBC, 25% solids, and pH 6. Chemical assays were obtained via ICP-OES.

Time (min)	Product	Mass recovery (%)	Mass recovery (SD)	Cu (%)	Cu (SD)	Fe (%)	Fe (SD)	Pb (%)	Pb (SD)	S (%)	S (SD)	Zn (%)	Zn (SD)
0.5	Concentrate	16.0	1.38	0.49	0.009	41.7	1.679	0.25	0.022	47.7	2.096	1.01	0.052
0.5	Tailing	84.0	1.38	0.33	0.009	25.4	0.417	0.36	0.023	22.7	0.946	0.65	0.011
1	Concentrate	24.6	2.10	0.49	0.012	41.5	1.522	0.25	0.024	47.3	1.771	1.02	0.066
1	Tailing	75.4	2.10	0.31	0.005	23.6	0.524	0.38	0.024	20.0	1.223	0.60	0.003
2	Concentrate	33.8	0.73	0.51	0.003	41.6	1.646	0.26	0.012	47.2	1.774	1.05	0.050
2	Tailing	66.2	0.73	0.27	0.012	21.1	0.021	0.39	0.028	16.2	0.619	0.53	0.003
4	Concentrate	45.1	0.48	0.51	0.004	40.5	1.178	0.28	0.013	45.6	1.292	1.08	0.048
4	Tailing	54.9	0.48	0.22	0.014	17.8	0.054	0.40	0.029	11.1	0.665	0.39	0.004
6	Concentrate	51.3	0.10	0.52	0.008	39.0	0.818	0.31	0.013	43.7	0.875	1.13	0.050
6	Tailing	48.7	0.10	0.19	0.016	15.8	0.179	0.41	0.031	7.6	0.590	0.29	0.009
8	Concentrate	54.8	0.10	0.51	0.008	39.1	0.819	0.31	0.014	43.5	0.873	1.08	0.050
8	Tailing	45.2	0.10	0.16	0.016	14.6	0.179	0.39	0.030	6.3	0.592	0.25	0.008
13	Concentrate	60.7	0.45	0.50	0.009	37.8	0.698	0.33	0.015	41.4	0.727	1.05	0.041
13	Tailing	39.3	0.45	0.12	0.018	13.0	0.364	0.36	0.031	4.0	0.440	0.17	0.005
16	Concentrate	63.3	0.52	0.49	0.011	37.0	0.588	0.34	0.019	40.2	0.648	1.02	0.042
16	Tailing	36.7	0.52	0.10	0.016	12.6	0.290	0.35	0.026	3.4	0.494	0.15	0.001

Time (min)	Product	Cu recovery (%)	Cu recovery (SD)	Fe recovery (%)	Fe recovery (SD)	Pb recovery (%)	Pb recovery (SD)	S recovery (%)	S recovery (SD)	Zn recovery (%)	Zn recovery (SD)
0.5	Concentrate	22.2	1.6	23.8	1.4	11.5	1.3	28.6	2.1	22.9	2.4
0.5	Tailing	77.8	1.6	76.2	1.4	88.5	1.3	71.4	2.1	77.1	2.4
1	Concentrate	34.4	2.7	36.4	2.3	18.0	2.1	43.5	3.4	35.6	4.2
1	Tailing	65.6	2.7	63.6	2.3	82.0	2.1	56.5	3.4	64.4	4.2
2	Concentrate	48.7	0.1	50.1	0.2	25.7	0.2	59.7	0.8	50.3	1.9
2	Tailing	51.3	0.1	49.9	0.2	74.3	0.2	40.3	0.8	49.7	1.9
4	Concentrate	65.9	0.9	65.1	0.3	36.9	0.2	77.1	0.9	69.4	1.6
4	Tailing	34.1	0.9	34.9	0.3	63.1	0.2	22.9	0.9	30.6	1.6
6	Concentrate	74.2	1.4	72.2	0.7	44.2	0.9	85.9	0.7	80.5	1.0
6	Tailing	25.8	1.4	27.8	0.7	55.8	0.9	14.1	0.7	19.5	1.0
8	Concentrate	80.0	1.4	76.4	0.7	49.5	0.9	89.3	0.7	84.2	1.0
8	Tailing	20.0	1.4	23.6	0.7	50.5	0.9	10.7	0.7	15.8	1.0
13	Concentrate	87.1	1.7	81.8	1.0	58.8	1.4	94.1	0.4	90.5	0.1
13	Tailing	12.9	1.7	18.2	1.0	41.2	1.4	5.9	0.4	9.5	0.1
16	Concentrate	89.1	1.5	83.5	0.8	62.8	1.0	95.4	0.5	91.9	0.1
16	Tailing	10.9	1.5	16.5	0.8	37.2	1.0	4.6	0.5	8.1	0.1

Fully liberated non-iron sulfides are present mostly in fine and ultrafine particles. They can be floated through true flotation but did not float as well as the grains associated with (coarser) pyrite.

The effect of size and liberation for Cu-, Zn-, and Pb-sulfide minerals shows a strong influence on the flotation performance. The coarser, more liberated material shows much faster flotation kinetics, better metal and sulfur recoveries, and cleaner residues than the finer material.

The recovery of the hydrophilic mineral groups increases with decreasing particle size and shows the effect of particle size on entrainment.

Classic bulk sulfide flotation of the coarser and finer fractions of the tailings in a two-step classification-flotation process results in the recovery of most of the sulfides (96.6% and 95.4%, respectively, in the coarser and finer fraction), a relatively sulfur-poor residue (1.6% and 3.4%, respectively, in the coarser and finer fractions), and a concentrate enriched in sulfur and base-metals (42.7% S, 0.62% Cu, 2.61% Zn, 0.40% Pb in the coarser fraction, and 40.2% S, 0.49% Cu, 1.02% Zn, 0.34% Pb in the finer fraction), compared to bulk flotation in a single step.

The addition of a flocculation step in the flotation of the fine particles increases the flotation kinetics and allows the generation of cleaner residues. However, it also increases the entrainment of hydrophilic particles and thus leads to a dilution of the concentrates.

The use of classic flotation produced tailings that represent 37–49% of the original mass but contain only 2.9–7.0% of the original sulfur (depending on the route utilized).

Overall, our results are very promising and show clear potential for further investigations on industrial applications. Particularly the classic two-step classification-flotation process opens potential avenues for industrial treatment routes which could increase the recovery of metals from the ores, reduce environmental hazards, and result in the potential utilization of a significant portion of the Neves-Corvo tailings in building materials.

CRediT authorship contribution statement

Ana Luiza Coelho Braga de Carvalho: Conceptualization, Methodology, Formal analysis, Investigation, Software, Data curation, Validation, Writing – original draft, Writing – review & editing, Visualization. **Victor Albuquerque de Carvalho:** Formal analysis, Investigation, Writing – review & editing, Visualization. **Rosie Blannin:** Software, Validation, Formal analysis, Data curation, Writing – review & editing, Visualization. **Alexandra Gomez Escobar:** Software, Validation, Formal analysis, Data curation, Writing – review & editing. **Max Frenzel:** Data curation, Validation, Writing – review & editing. **Martin Rudolph:** Data curation, Validation, Writing – review & editing. **André Carlos Silva:** Conceptualization, Writing – review & editing, Supervision. **Daniel Goldmann:** Conceptualization, Writing – review & editing, Supervision.

Declaration of Competing Interest

The authors declare that they have no known competing financial interests or personal relationships that could have appeared to influence the work reported in this paper.

Data availability

Data will be made available on request.

Acknowledgments

We would like to acknowledge the anonymous reviewers for their constructive comments and valuable insight. The company SOMINCOR Lundin Mining and Mafalda Oliveira for providing the tailings sample. Kai Bachmann (HZDR) is thanked for his support during SEM-MLA data acquisition. Petra Sommer (TU Clausthal), Heike Groβe (TU Clausthal), and Maike Gamenik (TU Clausthal) are acknowledged for performing the ICP-OES analysis. Sarah Tuchtfeld (TU Clausthal) for performing the particle size measurement. This research has received funding from the European Union's EU Framework Programme for Research and Innovation H2020 under grant agreement no 812580 (MSCA-ETN SULTAN).

Appendix A

Figs. A.1–A.3.

Appendix B

Table B.1.

Appendix C

Table C.1.

Appendix D

Table D.1.

Appendix E

Tables E.1–E.3.

References

Attia, Y.A., 1977. Development of a Selective Flocculation Process for a Complex Copper Ore. Int. J. Miner. Process. 4, 209–225. https://doi.org/10.1016/0301-7516(77)90003-5.

Babel, B., Penz, M., Schach, E., Boehme, S., Rudolph, M., 2018. Reprocessing of a Southern Chilean Zn Tailing by Flotation—A Case Study. Minerals 8, 295. https://doi.org/10.3390/min8070295.

Bachmann, K., Frenzel, M., Krause, J., Gutzmer, J., 2017. Advanced Identification and Quantification of In-Bearing Minerals by Scanning Electron Microscope-Based Image Analysis. Microsc. Microanal. 23, 527–537. https://doi.org/10.1017/S1431927617000460.

Benzaazoua, M., Bussière, B., Kongolo, M., McLaughlin, J., Marion, P., 2000. Environmental Desulphurization of Four Canadian Mine Tailings Using Froth Flotation. Int. J. Miner. Process. 60, 57–74. https://doi.org/10.1016/S0301-7516(00)00006-5.

Bevandić, S., Blannin, R., Gomez Escobar, A., Bachmann, K., Frenzel, M., Pinto, Á., Relvas, J.M.R.S., Muchez, P., 2022. Metal Deportment in Pb-Zn Mine Wastes from a Historic Tailings Pond, Plombières, East Belgium. Miner. Eng. 184, 107628 https://doi.org/10.1016/j.mineng.2022.107628.

Blannin, R., Frenzel, M., Tusa, L., Birtel, S., Ivăşcanu, P., Baker, T., Gutzmer, J., 2021. Uncertainties in Quantitative Mineralogical Studies Using Scanning Electron Microscope-Based Image Analysis. Miner. Eng. 167, 106836.

Bois, D., Poirier, P., Benzaazoua, M., Bussière, B., 2022. A Feasibility Study on the Use of Desulphurized Tailings to Control Acid Mine Drainage. 98, 361–380.

Boulton, A., Fornasiero, D., Ralston, J., 2001. Selective Depression of Pyrite with Polyacrylamide Polymers. Int. J. Miner. Process. 61, 13–22. https://doi.org/10.1016/S0301-7516(00)00024-7.

Cao, M., Liu, Q., 2006. Reexamining the Functions of Zinc Sulfate as a Selective Depressant in Differential Sulfide Flotation–the Role of Coagulation. J Colloid Interface Sci 301, 523–531. https://doi.org/10.1016/j.jcis.2006.05.036.

Demers, I., 2005. Enhancing Fine Particle Recovery in Flotation and its Potential Application to the Environmental Desulphurization Process. engd, Université du Québec en Abitibi-Témiscamingue: [Rouyn-Noranda], 2005.

Coelho Braga de Carvalho, A.L., Ludovici, F., Goldmann, D., Silva, A.C., Liimatainen, H., 2021. Silylated thiol-containing cellulose nanofibers as a bio-based flocculation agent for ultrafine mineral particles of chalcopyrite and pyrite. J. Sustain Metall. 7, 1506–1522. https://doi.org/10.1007/s40831-021-00439-y.

Escobar, A.G., Relvas, J.M.R.S., Pinto, Á.M.M., Oliveira, M., 2021. Physical-Chemical Characterization of the Neves Corvo Extractive Mine Residues: A Perspective Towards Future Mining and Reprocessing of Sulfidic Tailings. J. Sustain. Metall. 7, 1483–1505. https://doi.org/10.1007/s40831-021-00428-1.

Fandrich, R., Gu, Y., Burrows, D., Moeller, K., 2007. Modern SEM-Based Mineral Liberation Analysis. Int. J. Miner. Process. 84, 310–320. https://doi.org/10.1016/j.minpro.2006.07.018.

Frenzel, M., Bachmann, K., Carvalho, J.R.S., Relvas, J.M.R.S., Pacheco, N., Gutzmer, J., 2019. The Geometallurgical Assessment of By-Products—Geochemical Proxies for the Complex Mineralogical Deportment of Indium at Neves-Corvo, Portugal. Miner Deposita 54, 959–982. https://doi.org/10.1007/s00126-018-0849-6.

Gaspar, O., Pinto, Á., 1991. The Ore Textures of the Neves-Corvo Volcanogenic Massive Sulphides and Their Implications for Ore Beneficiation. 10.1180/MINMAG.1991.055.380.11.

Gaspar, O., 2002. Mineralogy and sulfide mineral chemistry of the neves–corvo ores, Portugal: Insight into their genesis. The Canadian Mineralogist 40, 611–636. https://doi.org/10.2113/gscanmin.40.2.611.

Gaudin, A.M.,1939. Principles of Mineral Dressing. McGraw-Hill Book Company, Incorporated; ISBN 978-0-07-023030-9.

Gong, J., Peng, Y., Bouajila, A., Ourriban, M., Yeung, A., Liu, Q., 2010. Reducing Quartz Gangue Entrainment in Sulphide Ore Flotation by High Molecular Weight Polyethylene Oxide. Int. J. Miner. Process. 97, 44–51. https://doi.org/10.1016/j.minpro.2010.07.009.

Gu, Y., 2003. Automated Scanning Electron Microscope Based Mineral Liberation Analysis An Introduction to JKMRC/FEI Mineral Liberation Analyser. J. Miner. Mater. Charact. Eng. 2, 33–41. https://doi.org/10.4236/jmmce.2003.21003.

Gupta, A., Yan, D.S., 2006. Mineral Processing Design and Operation: An Introduction. Elsevier, ISBN 978-0-08-045461-0.

Heinig, T., Bachmann, K., Tolosana-Delgado, R., Boogaart, G., Gutzmer, J., 2015. Monitoring gravitational and particle shape settling effects on MLA sample preparation.

Helser, J., Vassilieva, E., Cappuyns, V., 2022. Environmental and Human Health Risk Assessment of Sulfidic Mine Waste: Bioaccessibility, Leaching and Mineralogy. J. Hazard. Mater. 424, 127313 https://doi.org/10.1016/j.jhazmat.2021.127313.

Hoang, D.H., Kupka, N., Peuker, U.A., Rudolph, M., 2018. Flotation Study of Fine Grained Carbonaceous Sedimentary Apatite Ore – Challenges in Process Mineralogy and Impact of Hydrodynamics. Minerals Eng. 121, 196–204, 10.1016/j.mineng.2018.03.021.

Kamariah, N., Kalebic, D., Xanthopoulos, P., Blannin, R., Araujo, F., Koelewijn, S.-F., Dehaen, W., Binnemans, K., Spooren, J., 2022. Conventional versus Microwave-Assisted Roasting of Sulfidic Tailings: Mineralogical Transformation and Metal Leaching Behavior. Miner. Eng. 183, 107587 https://doi.org/10.1016/j.mineng.2022.107587.

Kern, M., Möckel, R., Krause, J., Teichmann, J., Gutzmer, J., 2018. Calculating the Deportment of a Fine-Grained and Compositionally Complex Sn Skarn with a Modified Approach for Automated Mineralogy. Miner. Eng. 116, 213–225. https://doi.org/10.1016/j.mineng.2017.06.006.

Leistner, T., Embrechts, M., Leißner, T., Chehreh Chelgani, S., Osbahr, I., Möckel, R., Peuker, U.A., Rudolph, M., 2016. A Study of the Reprocessing of Fine and Ultrafine Cassiterite from Gravity Tailing Residues by Using Various Flotation Techniques. Miner. Eng. 96–97, 94–98. https://doi.org/10.1016/j.mineng.2016.06.020.

Lu, S., Pugh, R.J., Forssberg, E. (Eds.), 2005. Chapter 7 Flocculation with polymers. Studies in Interface Science, Interfacial Separation of Particles. Elsevier, pp. 354–414.

Mandre, N.R., Panigrahi, D., 1997. Studies on selective flocculation of complex sulphides using cellulose xanthate. Int. J. Miner. Process. 50, 177–186. https://doi.org/10.1016/S0301-7516(97)00013-6.

Martins, N.P., Srivastava, S., Simão, F.V., Niu, H., Perumal, P., Snellings, R., Illikainen, M., Chambart, H., Habert, G., 2021. Exploring the Potential for Utilization of Medium and Highly Sulfidic Mine Tailings in Construction Materials: A Review. Sustainability 13, 12150. https://doi.org/10.3390/su132112150.

Mweene, L., Subramanian, S., 2018. Selective Dispersion-Flocculation and Flotation Studies on a Siliceous Copper Ore. Physicochem. Probl. Miner. Process. 54, 1282–1291. https://doi.org/10.5277/ppmp18186.

Nadeif, A., Taha, Y., Bouzahzah, H., Hakkou, R., Benzaazoua, M., 2019. Desulfurization of the Old Tailings at the Au-Ag-Cu Tiouit Mine (Anti-Atlas Morocco). Minerals 9, 401. https://doi.org/10.3390/min9070401.

Niu, H., Adrianto, L., Escobar, A., Zhukov, V., Perumal, P., Kauppi, J., Kinnunen, P., Illikainen, M., 2021. Potential of Mechanochemically Activated Sulfidic Mining Waste Rock for Alkali Activation. J. Sustain. Metall. 7 https://doi.org/10.1007/s40831-021-00466-9.

Nogueira, F.C., 2019. Agregação hidrofóbica aplicada ao beneficiamento de finos de minério de ferro. Universidade Federal de Ouro Preto.

Oliveira, M., 2019. Gestão de Residuos Mineiros Neves Corvo Mine. Universidade de Lisboa.

Oliveira, M.F.M. de, 2016. Poliacrilamidas na flotação catiônica reversa de minério de ferro.

Opara, C.B., Kutschke, S., Pollmann, K., 2022. Fractionation of Metal(Loid)s in Three European Mine Wastes by Sequential Extraction. Separations 9, 67. https://doi.org/10.3390/separations9030067.

Parbhakar-Fox, A., Lottermoser, B., Hartner, R., Berry, R.F., Noble, T.L., 2017. Prediction of Acid Rock Drainage from Automated Mineralogy. In: Lottermoser, B. (Ed.), Environmental Indicators in Metal Mining. Springer International Publishing, Cham, 2017, pp. 139–156 ISBN 978-3-319-42731-7.

Pereira, L., Frenzel, M., Hoang, D.H., Tolosana-Delgado, R., Rudolph, M., Gutzmer, J., 2021. Computing Single-Particle Flotation Kinetics Using Automated Mineralogy Data and Machine Learning. Miner. Eng. 170, 107054 https://doi.org/10.1016/j.mineng.2021.107054.

Pereira, L., Frenzel, M., Khodadadzadeh, M., Tolosana-Delgado, R., Gutzmer, J., 2021. A Self-Adaptive Particle-Tracking Method for Minerals Processing. J. Clean. Prod. 279, 123711 https://doi.org/10.1016/j.jclepro.2020.123711.

Relvas, J., 2000. Geology and Metallogenesis at the Neves Corvo Deposit. Faculdade de Ciências da Universidade de Lisboa, Portugal.

Relvas, J.M.R.S., Barriga, F.J.A.S., Pinto, Á., Ferreira, A., Pacheco, N., Noiva, P., Barriga, G., Baptista, R., Carvalho, D. de, Oliveira, V., et al., 2002. The Neves-Corvo Deposit, Iberian Pyrite Belt, Portugal: Impacts and Future, 25 Years after the Discovery. 10.5382/SP.09.08.

Relvas, J.M.R.S., Barriga, F.J.A.S., Ferreira, A., Noiva, P.C., Pacheco, N., Barriga, G., 2006. Hydrothermal Alteration and Mineralization in the Neves-Corvo Volcanic-Hosted Massive Sulfide Deposit, Portugal. I. Geology, Mineralogy, and Geochemistry. Econ. Geol. 101, 753–790, 10.2113/gsecongeo.101.4.753.

Römer, F., Binder, A., Goldmann, D., 2018. Basic Considerations for the Reprocessing of Sulfidic Tailings Using the Example of the Bollrich Tailing Ponds. World Metall. - ERZMETALL 71.

Rubio, J., Marabini, A.M., 1987. Factors Affecting the Selective Flocculation of Hydroxyapatite from Quartz and/or Calcite Mixtures. Int. J. Miner. Process. 20, 59–71. https://doi.org/10.1016/0301-7516(87)90017-2.

Schueler, T.A., de Aguiar, P.F., Vera, Y.M., Goldmann, D., 2021. Leaching of Cu, Zn, and Pb from Sulfidic Tailings Under the Use of Sulfuric Acid and Chloride Solutions. J. Sustain. Metall. 7, 1523–1536. https://doi.org/10.1007/s40831-021-00446-z.

Simão, F.V., Chambart, H., Vandemeulebroeke, L., Nielsen, P., Cappuyns, V., 2021. Turning Mine Waste into a Ceramic Resource: Plombières Tailing Case. J. Sustain. Metall. 7, 1469–1482. https://doi.org/10.1007/s40831-021-00442-3.

Sivamohan, R., 1990. The Problem of Recovering Very Fine Particles in Mineral Processing — A Review. Int. J. Miner. Process. 28, 247–288. https://doi.org/10.1016/0301-7516(90)90046-2.

Skandrani, A., Demers, I., Kongolo, M., 2019. Desulfurization of Aged Gold-Bearing Mine Tailings. Miner. Eng. 138, 195–203. https://doi.org/10.1016/j.mineng.2019.04.037.

Somasundaran, P., 1978. Selective flocculation of fines. Phys. Chem. Mineral-Reagent Interactions in Sulfide Flotation, Bureau of Mines, pp. 150–167.

Somasundaran, P., Ren, Y., Rao, M.Y., 1998. Applications of Biological Processes in Mineral Processing. Colloids Surf A Physicochem Eng Asp 133, 13–23. https://doi.org/10.1016/S0927-7757(97)00173-8.

Sresty, G.C., Somasundaran, P., 1980. Selective Flocculation of Synthetic Mineral Mixtures Using Modified Polymers. Int. J. Miner. Process. 6, 303–320. https://doi.org/10.1016/0301-7516(80)90027-7.

Trahar, W.J., Warren, L.J., 1976. The Flotability of Very Fine Particles — A Review. Int. J. Miner. Process. 3, 103–131. https://doi.org/10.1016/0301-7516(76)90029-6.

Veiga Simão, F., Chambart, H., Vandemeulebroeke, L., Cappuyns, V., 2021. Incorporation of Sulphidic Mining Waste Material in Ceramic Roof Tiles and Blocks. J. Geochem. Explor. 225, 106741 https://doi.org/10.1016/j.gexplo.2021.106741.

Wang, L., 2013. The Use of Polyacrylamide as a Selective Depressant in the Separation of Chalcopyrite and Galena. University of Alberta. Master Thesis,.

Wang, D., Liu, Q., 2021. Hydrodynamics of Froth Flotation and Its Effects on Fine and Ultrafine Mineral Particle Flotation: A Literature Review. Miner. Eng. 173, 107220 https://doi.org/10.1016/j.mineng.2021.107220.

Wang, D., Liu, Q., 2021. Influence of Aggregation/Dispersion State of Hydrophilic Particles on Their Entrainment in Fine Mineral Particle Flotation. Miner. Eng. 166, 106835 https://doi.org/10.1016/j.mineng.2021.106835.

Wang, L., Peng, Y., Runge, K., Bradshaw, D., 2015. A Review of Entrainment: Mechanisms, Contributing Factors and Modelling in Flotation. Miner. Eng. 70, 77–91. https://doi.org/10.1016/j.mineng.2014.09.003.

Wightman, E.M., Grano, S.R., Ralston, J., 2000. Selectivity in the Polymer Assisted Separation of Galena from Quartz by Flotation. Miner. Eng. 13, 843–856. https://doi.org/10.1016/S0892-6875(00)00073-X.

Wills, B.A., Finch, J.A., 2016. Froth Flotation. In: Wills' Mineral Processing Technology. Elsevier, pp. 265–380. ISBN 978-0-08-097053-0.